# 3. RESULTS

## 3.1 SCYL1BP1 is a new member of Golgi-resident proteins

### 3.1.1 Preparing polyclonal and monoclonal antibodies

Porostin (SCYL1BP1; POST) is a protein with largely unknown function, although two interaction partners were reported (Di et al., 2003; Zhang et al., 2005). To raise polyclonal antibody (Ab) against Porostin, two peptides chosen from human protein sequence were synthesized and then used as antigen for immunization in rabbit (**Fig. 1**). This was done by a commercial provider (Eurogentec). After three months, anti-serum was harvested, and purified by peptide conjugated beads for later use.

Through a collaboration with the Deutsches Krebsforschungszentrum (DKFZ), screening for monoclonal Abs against Porostin was performed. The antigen used for immunization arose from the labelled part of mouse protein expressed by pET-30b(+) in E. coli (**Fig. 1**). To screen for positive clones, the culture medium in which the hybridoma cells had been maintained was harvested and directly applied to the test by immunofluorescence approach in chicken fibroblasts infected by RCAS-mPOST-Flag virus.

### 3.1.2 Verifying polyclonal and monoclonal antibodies

Since the exogenous expression of Porostin driven by pCMV-Flag–5a (Sigma) produced drastic effects such as nuclear breakdown and fibre formation (data not shown), we therefore decided to establish a system that would allow a lower level of expression of Porostin by RCAS retrovirus in chicken cells. In contrast to transient transfection, only one copy of the retrovirus is introduced in the genome of the infected cell.

Using Forward and Reverse primers which cover the start codon of murine Scyl1bp1 and Flag-Tag respectively, we generated one PCR product corresponding to full length of murine Scyl1bp1 including Flag Tag in its C-terminal based on pCMV-mPOST-Flag–5a (**Fig. 2a**). Ligation was then performed between A-tailed Scyl1bp1-Flag and T-tailed linearized RCAS vector generated by SwaI digestion. Positive clones growing on Amp-LB growth plates were screened by PCR followed by confirmation by sequencing (**Fig. 2a**). Positive constructs were then transfected into avian DF1 cell line for virus production.

Human SCYL1BP1

```
        10          20          30          40          50          60
MSWAAVLAVA AARFGHFWGC RWPGPMAQGW AGFSEEELRR LKQTKDPFEP QRRLPAKKSR

        70          80          90         100         110         120
QQLQREKALV EQSQKLGLQD GSTSLLPEQL LSAPKQRVNV QKPPFSSPTL PSHFTLTSPV

       130         140         150         160         170         180
GDGQPQGIES QPKELGLENS HDGHNNVEIL PPKPDCKLEK KKVELQEKSR WEVLQQEQRL

       190         200         210         220         230         240
MEEKNKRKKA LLAKAIAERS KRTQAETMKL KRIQKELQAL DDMVSADIGI LRNRIDQASL

       250         260         270         280         290         300
DYSYARKRFD RAEAEYIAAK LDIQRKTEIK EQLTEHLCTI IQQNELRKAK KLEELMQQLD

       310         320         330         340         350         360
VEADEETLEL EVEVERLLHE QEVESRRPVV RLERPFQPAE ESVTLEFAKE NRKCQEQAVS

       370         380         390
PKVDDQCGNS SSIPFLSPNC PNQEGNDISA ALAT
```

EP060752 & EP060753 Antigen of immunization for raising polyclonal Ab in rabbit
M: the real start of translation

Mouse SCYL1BP1

```
        10          20          30          40          50          60
MAQDWAGFSE EELRRLKQNK DPFEPQRRIP VKKTRQQLQR EKALLEQSQK LGLQDGSASL

        70          80          90         100         110         120
LPEQLLSAPK QRANSQKPRS PSPVAPSPLT PTSSSGDGKL PGVGSQPQEP GLENSHHGHK

       130         140         150         160         170         180
SAEVRAPKPD CKVEKKKMEL QEKSRWEVLQ QEQRLMEEKN KRKKALLAQA IAERSKKTQA

       190         200         210         220         230         240
ETIKLKRIQK ELQALDDMVS ADIGILRNRI DQASLEYSYA RKRFDRAEAE YITAKLDLQR

       250         260         270         280         290         300
KTETKEQLTE HLCTIIQQNE LRKAKKLEEL MQQLDVQADE EALQLEVEVE QLLREQEAEA

       310         320         330         340         350         360
AKQMASVERL CPPDGESVSS ELAEENNEPQ KQAPSPETDK PGKCCSSSPH RLDCPDPGAK

     368
NFSAAVAT
```

Antigen of Immunization used for raising monoclonal Ab in rat hybridoma

**Fig. 1.** The Antigen of immunization for antibody preparation. Two peptides in human protein, EP060752 & EP060753, labelled by red and green respectively, were synthesized as antigens for polyclonal antibody preparation in rabbit. One fragment that was red labelled in mouse protein was expressed by PET-30b as an antigen for raising monoclonal antibody in rat hybridoma.

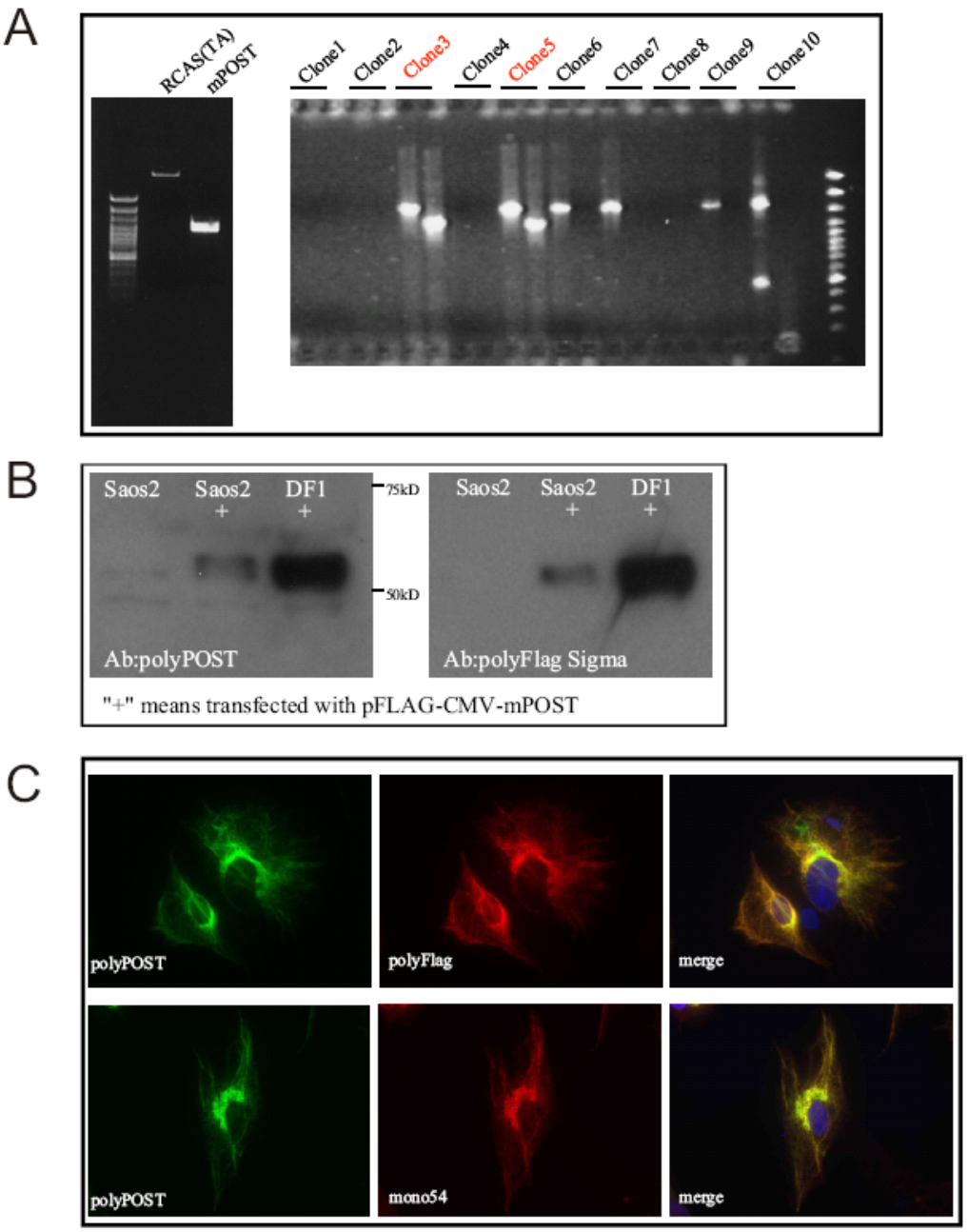


**Fig. 2.** Antibody verification. (A) To establish a system for monoclonal antibody screening, RCAS-mPOST (murine Scyl1bp1) was constructed for retrovirus production which drives expression of mPOST-Flag. (B) Using anti-Flag antibody (polyclonal from Sigma) as a positive Ctl, application of polyclonal antibody against Porostin was verified in Western blot. (C) By immunofluorescence approach, polyclonal antibody and one monoclonal antibody (#54) recognized the same signal as anti-Flag antibody in primary chicken fibroblasts infected by RCAS-mPOST virus.

By immunofluorescence approach, we tested the anti-Porostin polyclonal Ab and screened for some monoclonal Abs by viewing subcellular co-localization with anti-Flag Ab in primary chicken fibroblasts which had been infected by RCAS-mPOST-Flag virus. 11 out of 64 monoclonal Abs as well as polyclonal Ab against Porostin were identified to produce the same subcellular pattern as anti-Flag Ab (**Fig. 2c**) and signal intensity of different mono-clones was indicated (**Table 1**). Importantly, by Western blot, polyclonal Ab and anti-Flag Ab recognized the same band, which should correspond to overexpressed Porostin (**Fig. 2b**). Unfortunately, we did not observe any of monoclonal Abs recognizing this band (**Table 1** and data not shown).

| The number of clones tested by IF | Positive clones by IF | The number of clones tested by blot | Positive clones by blot |
|---|---|---|---|
| 64 | 11 | 11 | 0 |

| The No. | #13 | #54 | #60 | #61 | #64 | #79 | #97 | #108 | #110 | #113 | #121 |
|---|---|---|---|---|---|---|---|---|---|---|---|
| Signal | ++ | +++ | + | + | + | + | + | + | ++ | + | + |

**Table 1.** The monoclonal antibody screening. By immunofluorescence (IF) approach in primary chicken fibroblasts infected by RCAS-mPOST, we screened for positive clones against Porostin. We directly applied the medium collected from different clones of monoclonal antibody to fixed cells after blocking with 3% BSA. Totally, 11 out of 64 clones were identified to be positive and several subclones of each were subsequently used for confirmation (upper panel). These 11 clones were also tested by Western blot, however, none of them turned out to be effective. The intensity of IF signal was indicated by "+", and #54 clone gave the strongest signal (lower panel).

### 3.1.3 Subcellular localization

After verifying our anti-Porostin antibodies by anti-Flag antibody in Porostin-overexpressing cells, we started to address the subcellular localization of endogenous Porostin in primary human fibroblasts by immunofluorescence approach. As shown in (**Fig. 3**), we detected some ribbon-like signal in the cytoplasm of Ctl cells, which was absent in all our GO patient cells harboring different mutations in the gene Scyl1bp1. This result indicated that mutated forms of Porostin are not present in the patient cells. The failure to detect Porostin in one patient from Oman with Met26Leu mutation supports our notion that the second ATG, but not the first ATG of human cDNA of Scyl1bp1 is the real start codon in use. Since the Met26 residue is not residing in the epitopes used for immunization the loss of the fluorescence signal in the patient cells can only be explained by a loss of expression.

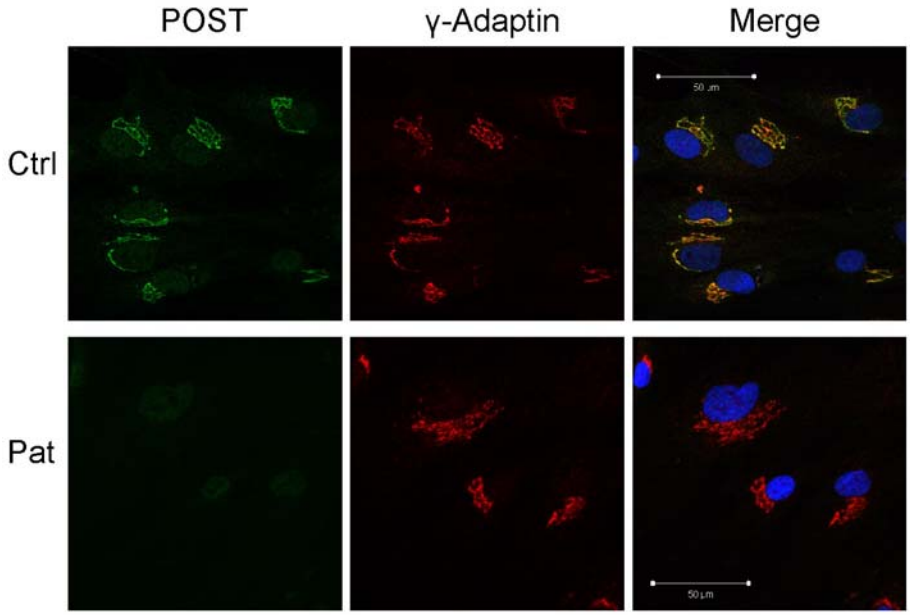


**Fig. 3.** Porostin is a Golgi resident protein. Using γ-Adaptin as a Golgi marker, we could observe co-localized signal between Porostin and γ-Adaptin in Ctl HAF (upper panel), by contrast, only γ-Adaptin was present in all our GO patient HAF (lower panel).

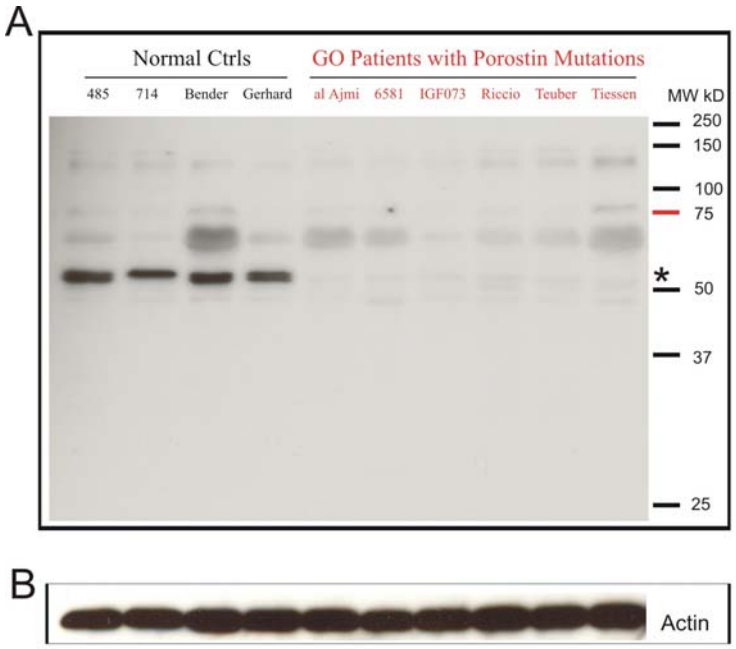


**Fig. 4.** Porostin protein was depleted in all GO patients. (A) Using polyclonal antibody against Porostin, we detected one band (~52kD), indicated by asterisk (⋆), corresponding to Porostin in all normal HAF tested. By contrast, such a band was not detected in GO patients regardless of any mutations in Scyl1bp1. The patient al Ajmi harbors homozygous Met26Leu mutation in Scyl1bp1. (B) Antibody against Actin was used in the experiment as a loading Ctl.

### 3.1.4 Western blot in primary human fibroblasts

The result from Western blot provided additional evidence for our presumption that loss of function of Porostin contributes to GO syndrome. All four normal Ctl samples exhibited one strong band corresponding to endogenous Porostin as indicated by positive Ctl, however, no such a band or lower band was detected in patient samples, indicating the absence of any truncated forms of protein (**Fig. 4**). The band was also lost in the patient with Met26Leu mutation, consistent with the immunofluorescence result, supporting the assumption that the Met26Leu mutation affects the start codon, thereby preventing the initiation of protein translation. Notably, in denaturing SDS-PAGE gel, Porostin had a MW around 52 kD, much bigger than predicated 42 kD of MW. It might be due to multiple phosphorylation and/or other post-translational modification (e.g. glycosylation) in its mature form.

### 3.1.5 Co-localization of SCYL1BP1 with Golgi markers

To further define the subcellular pattern of SCYL1BP1 in human fibroblasts, we employed several molecular markers including ER marker PDI, Golgi marker γ- Adaptin as well as cytoskeleton markers including Actin, Tubulin and Vimentin. As shown in (**Fig. 3**), Porostin displayed the best colocalization with the trans-Golgi marker γ-Adaptin. The fluorescence signals were closely adjacent even though this colocalization was incomplete as indicated by the incomplete yellow signals. Thus, we conclude that Porostin resides in the organelle: the Golgi apparatus.

To characterize the subdomains of the Golgi apparatus where Porostin resides, we performed co-staining of Porostin with trans-Golgi marker TGN46 and cis-Golgi marker GM130. Some other Golgi resident proteins including AKAP450 and GMAP210 were also tested. The result demonstrated that Porostin colocalized partially with all of the trans-Golgi markers, however, complete colocalization was not observed in any case (**Fig. 5**). Not until examining the overlap between Porostin and Rab6, was Porostin clearly defined to the medial and trans Golgi domains (**Fig. 18e**).

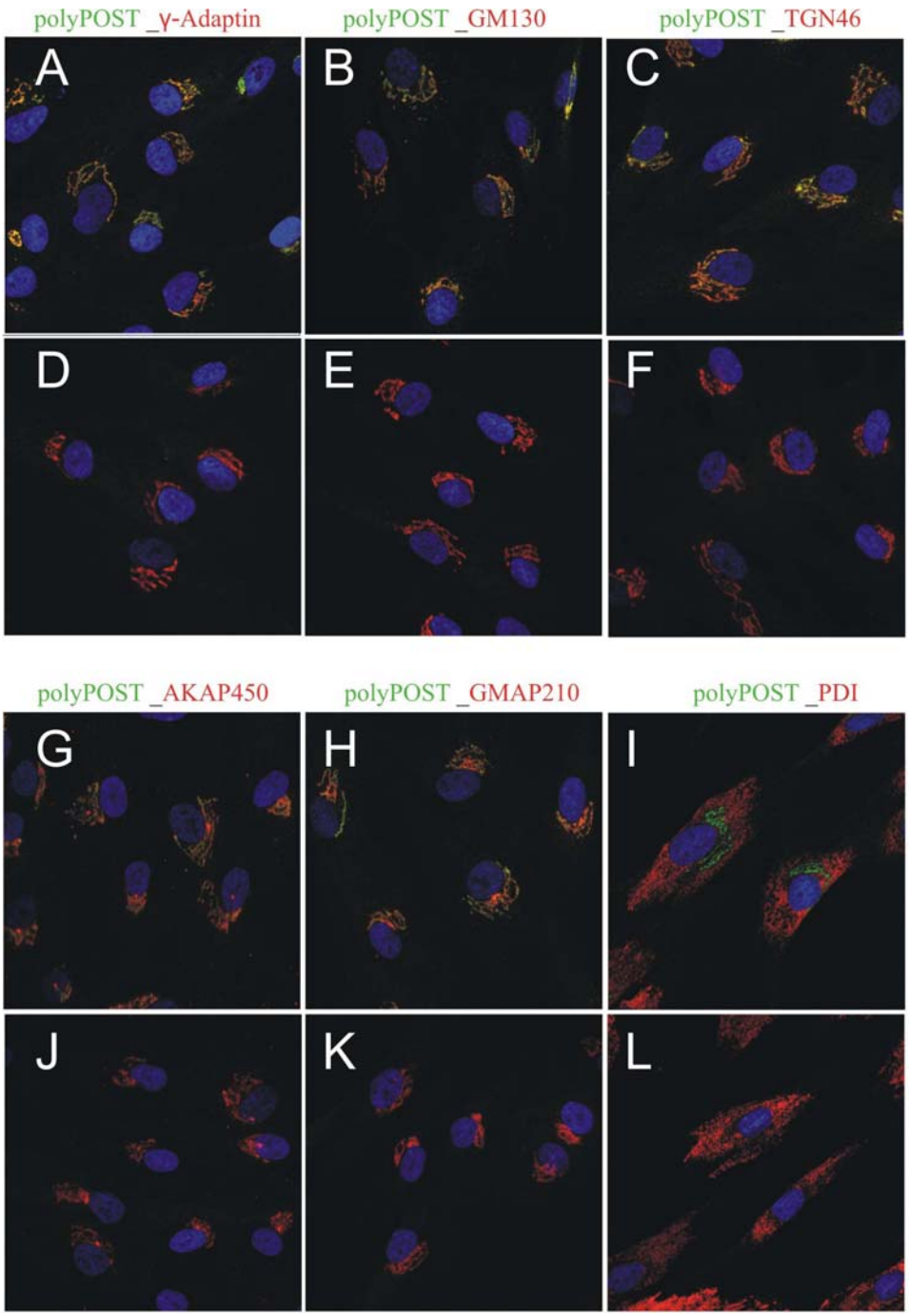


**Fig. 5.** Porostin colocalizes with multiple Golgi markers. (A,B,C,G,H) Colocalized signal between Porostin and Golgi markers was seen in normal HAF cells. (D,E,F,J,K) Whereas Porostin protein was depleted in all patient HAF cells, none of Golgi markers was affected by loss of Porostin protein. (I,L) PDI, one ER marker did not show any colocalization with Porostin in normal HAF cells (I), with patient HAF cells as a negative Ctl (L). The best overlap was seen with trans-Golgi markers γ-Adaptin and TGN46.

### 3.1.6 Response of SCYL1BP1 to Brefeldin A and Nocodazole

Brefeldin A (BFA) is a fungal metabolite synthesized by some organisms such as *Eupenicillium brefeldianum*. The BFA's utility for cell biologists began in the late 1980s,

when the block of protein secretion was observed upon treatment. In BFA treated cells, the inhibition occurred in the early step of the secretory pathway since the secretory and membrane proteins were retained in the ER. By interfering with anterograde transport of proteins into post-Golgi compartments, BFA induces redistribution of Golgi resident proteins, leading to the disassembly of the Golgi apparatus. Nocodazole (NZ) is another drug frequently used to characterize Golgi proteins. NZ exerts its effect by depolymerizing microtubules, thereby causing Golgi dispersal. The effects both BFA and NZ exert on Golgi morphology in short term can be completely reversed by removing the drugs, however, long term incubation with BFA (e.g. overnight) leads cell to apoptosis.

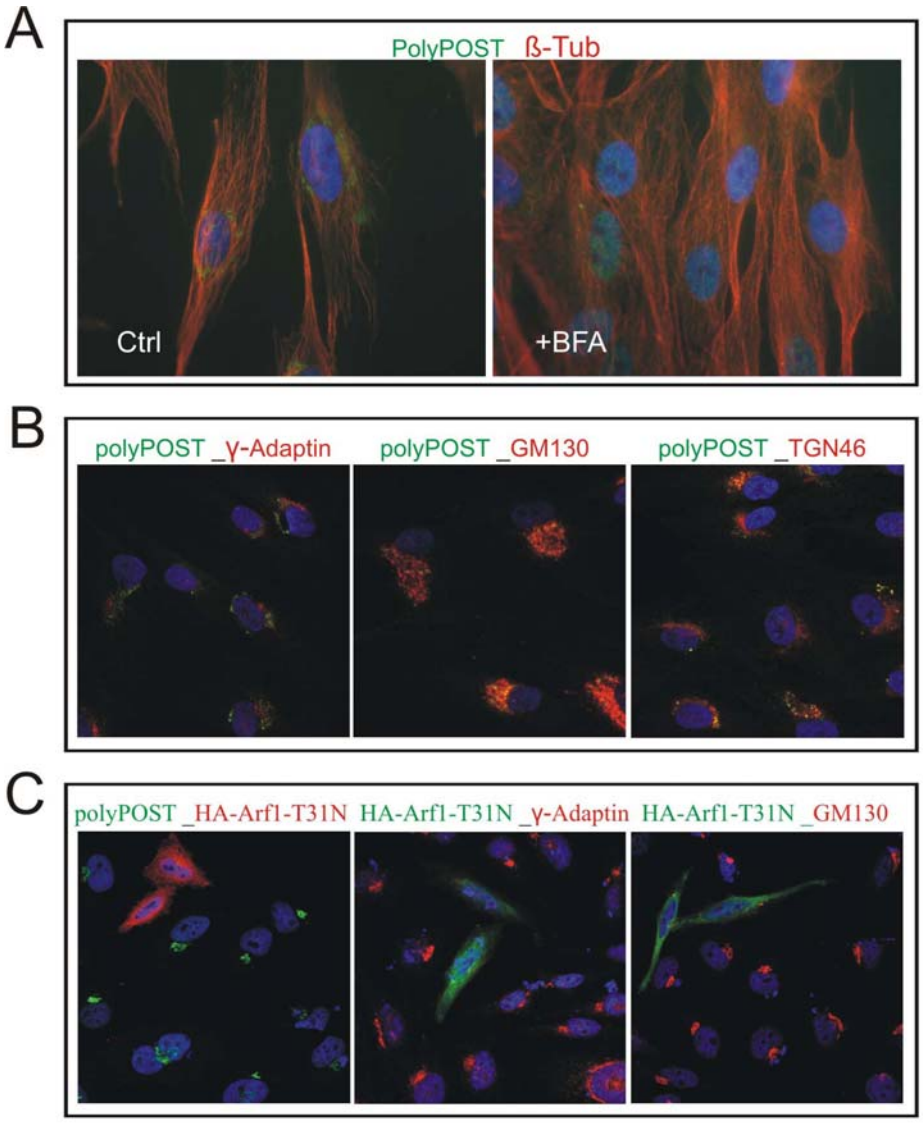


**Fig. 6.** Sensitivity of Porostin to BFA treatment. (A) As short as 6 min after BFA treatment, Porostin scattered around the cytoplasm. (B) The redistribution of Golgi was evident by Golgi markers: γ-Adaptin, GM130 and TGN46. (C) The effect of BFA was mimicked by expressing one dominant negative form of

Arf1-T31N.

Here we applied BFA and NZ in human primary fibroblasts to address the reaction of Porostin to these compounds. Our result showed that Porostin was rapidly scattered throughout the cytoplasm within 6min of exposure to 5 μg/ml BFA in most cells (**Fig. 6a,b**). With a bit longer incubation (e.g. 15 min), Porostin was only detected with diminishing signal, and even vanished in some cells. After 2 h incubation with 10 μM NZ, Porostin was redistributed in punctate clusters, in which other Golgi proteins such as γ-Adaptin and GM130 also resided (**Fig. 7b**), therefore these clusters were actually fractions of the Golgi apparatus. Dispersed Porostin did not show any colocalization with PDI, one ER marker (**Fig. 7b**). Placing the cells in fresh medium after removing BFA and NZ caused the cells to completely recover and the ribbon-like signal reappeared.

### 3.1.7 Response of SCYL1BP1 to mutant form of Arf1

Arf1 (ADP-ribosylation factor 1), one GTPase of Ras superfamily plays a crucial role in vesicle formation in yeast as well as in higher eukaryotes. It is thought that BFA exerts its effect at least in part by the inactivation of Arf1, therefore blocking secretory pathway and causing Golgi disassembly. We used the GDP locked form of ARF1-T31N (a kind gift from Dr. Juan S. Bonifacino), which fails to bind to cellular membranes, to address the response of SCYL1BP1 to this mutant form of Arf1 (Boehm et al., 2001; Ooi et al., 1998). As shown in (**Fig. 6c**), Porostin was dispersed in ARF1-T31N expressing cells, with as low intensity of signal as in BFA treated cells (**Fig. 6a,c**).

In Summary, by employing different markers, we could classify SCYL1BP1 to one new member of Golgi proteins. The utilization of BFA and NZ addressed the sensitivity of this new member to these drugs. Importantly, the response of SCYL1BP1 to BFA treatment was similarly stimulated by expressing one dominant negative mutant of ARF1-T31N in cells.

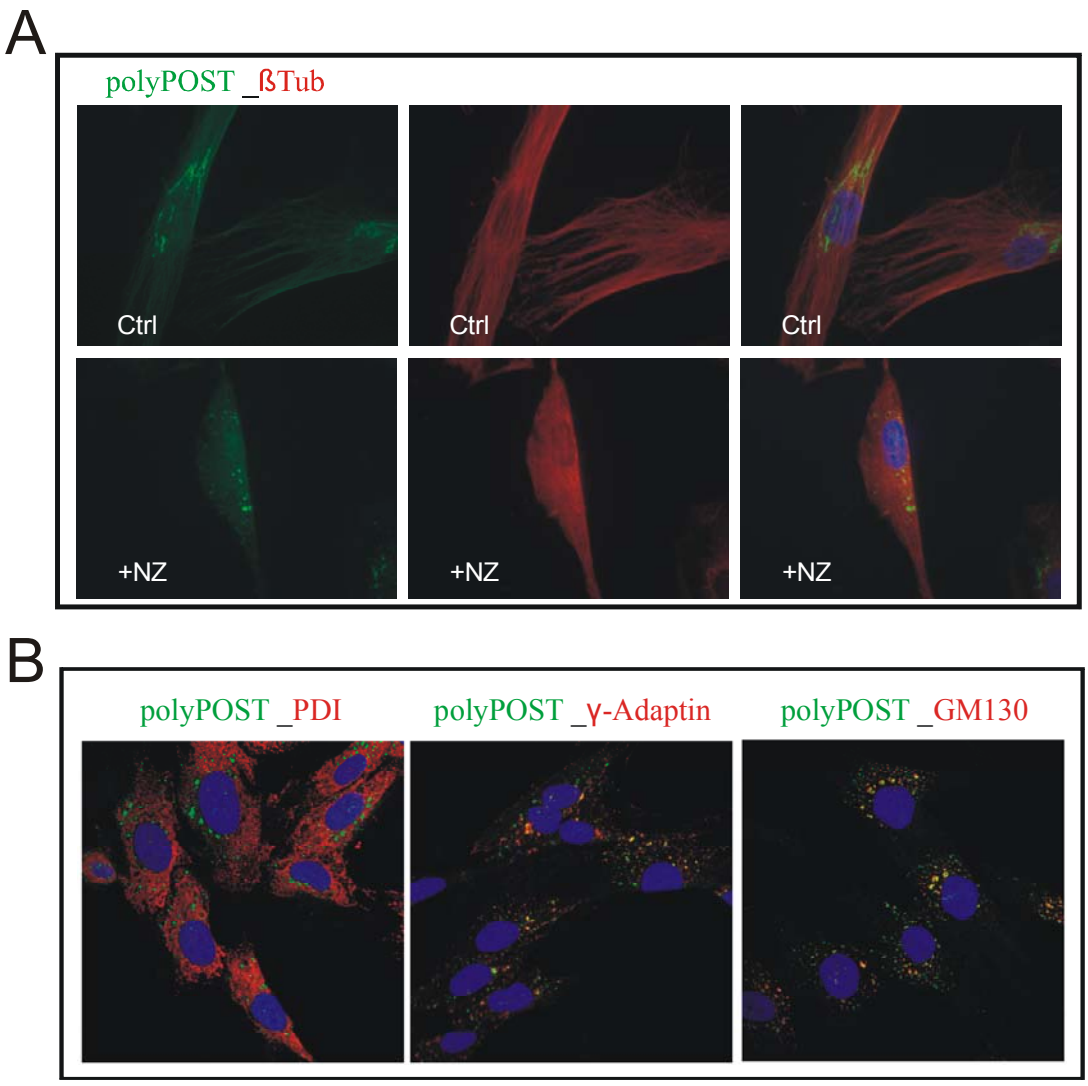


**Fig. 7.** NZ treatment caused redistribution of Porostin. (A) NZ exerts its effect by depolymerizing microtubules. Two hour incubation with 10 µM NZ redistributed Porostin in punctate clusters. (B) In NZ treated cells, Porostin clustered together with some Golgi proteins such as γ- Adaptin and GM130 (middle and right panels). No colocalization between these clusters and PDI, one ER marker, was observed (left panel).

## 3.2 Generation and characterization of gene-trap mice

### 3.2.1 Gene trap ES cell line

To generate a mouse model for functional investigation of Porostin, a BLAST search was performed in the database of The International Gene Trap Consortium (IGTC, http://www.genetrap.org/). One cell line called XG183 at BayGenomics, UCSF, was claimed to have trapped the gene. The sequencing chromatogram provided by BayGenomics implied that the insertion of pGT1Lxf, one gene trap vector, occurred within intron 1 of Scyl1bp1. Predictably, the normal SCYL1BP1 protein in this cell line was replaced by altered chimera, which only carries the first 20 aa of SCYL1BP1, and therefore it is very likely to create a null allele.

Gene trapping is a high-throughput approach that is used to introduce insertional mutations across the genome in mouse embryonic stem (ES) cells by gne trap vectors that simultaneously mutate and report the expression of the endogenous gene at the site of insertion and provide a DNA tag for the rapid identification of the disrupted gene. The mutant mice generated from ES cell lines carrying gene trap insertions could be applied to large-scale functional analysis of mammalian genes.

To confirm the cDNA fusion between Scyl1bp1 exon 1 and pGT1Lxf exon in the ES cells of XG183, we designed forward primers from exon1 of Scyl1bp1 (Flj-elfERV, Flj-BEIF, Flj-BHIF), with one primer from exon 2 (Flj-e2f) as negative Ctl. GT-vec-βGeo-R1 from pGT1Lxf exon region was used as Reverse primer. After reverse transcribing total RNA of XG183 ES cells into cDNA, we made a PCR with template cDNA. As expected, one band was detected at 400 bp, corresponding to the fused cDNA product between Scyl1bp1 Exon 1 and pGT1Lxf exon (**Fig. 8a**). By contrast, forward primer from exon 2 did not give rise to this product (**Fig. 8a**). This result demonstrated that only exon 1 of Scyl1bp1 is incorporated into the recombined mRNA in XG183 ES cells. In addition, only one copy of insertion was revealed in the genome by Southern blot (data not shown).

### 3.2.2 Generation of gene trap mouse

After confirmation of the altered Scyl1bp1 locus, the cultured ES cells of XG183 were injected into blastocysts; the ES cells were incorporated into the growing embryo, which

was then introduced into pseudopregnant mouse. The mice produced by these injected embryos carry the mutant gene in some somatic cells, which we call founder chimeras. After breeding with wild type (WT) mice, the founder chimeras with alteration in germ-line cells generate some progeny with one mutated allele in all cells, which we call heterozygotes. Such two of these heterozygotes are in turn bred, then some of the progeny contain two altered alleles in all of their cells, which we call homozygotes.

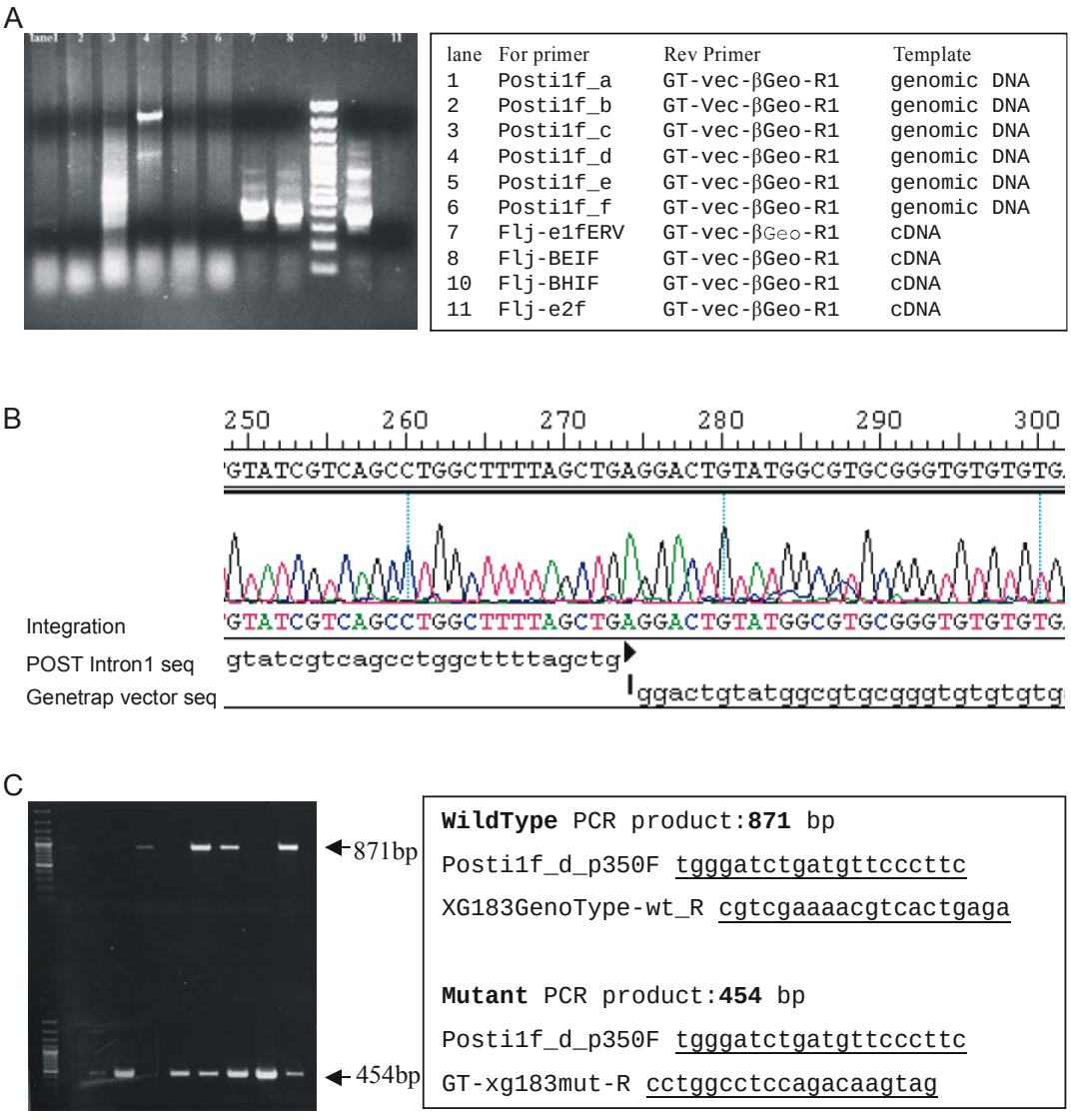


**Fig. 8.** Fine mapping of the gene trap insertion site of the XG183 mouse line. (A) PCR confirmed the insertion of gene trap vector into the genome of Xg183 cells. (B) By sequencing we identified the exact region where the intron 1 of Scyl1bp1 was interrupted by the insertion of Gene trap vector pGT1Lxf. Sequencing template arose from purified PCR product from lane 4 of (A); Sequencing primer is Posti1f_d_P350f. (C) PCR strategy for genotyping. By using the same forward primer combined with different reverse primers, 871 bp PCR product arose from WT allele; 454 bp PCR product arose from mutant allele.

### 3.2.3 Mapping the insertion site

For fine mapping the exact position where pGT1Lxf was inserted into the genome, we scanned intron 1 by placing primers every 1000 bp as Posti1f_a, Posti1f_b, Posti1f_c, Posti1f_d, Posti1f_e, Posti1f_f. GT-vec-βGeo-R1 was used as reverse primer. Genomic DNA from these ES cells served as PCR template. As shown in lane 4 of (**Fig. 8a**), one PCR product around 2.5 kb was amplified by Posti1f_d. By sequencing this product from both 5' and 3' ends, we revealed the location of Scyl1bp1 intron 1 at 5' end, and exon part of pGT1Lxf at the other end. Because the recombination site was not reachable by this sequencing, we designed a few primers downstream of Posti1f_d, including Posti1f_d_P350f and Posti1f_d_P570f. According to the sequencing data produced by Posti1f_d_P350f, the insertion site was finally mapped, as shown in (**Fig. 8b**), intron 1 of Scyl1bp1 was recombined with pGT1Lxf.

### 3.2.4 Genotyping

Based on the positional information of the insertion in the mouse genome, we designed PCR primers in order to distinguish between WT and mutant alleles by PCR. For WT genotyping, the forward primer is located before the insertion site; whereas the reverse primer recognizes the sequence after the insertion site. For mutant genotyping, the same forward primer was used, however, reverse primer was chosen from pGT1Lxf intron, which is excluded from WT. The favourable length of both PCR products is expected to range from 300 bp to 1000 bp. After doing PCR at different conditions, the optimized program was fixed for later genotyping. As shown in (**Fig. 8c**), WT showed one band corresponding to predicted 871 bp, by contrast, mutant gave rise to one product, consistent with predicted size of 454 bp.

### 3.2.5 Analysis of Scyl1bp1 expression

To investigate the effect of the gene trap insertion into the scyl1bp1 gene we analyzed gene expression. Mouse embryonic fibroblasts (MEF) were isolated from E13.5 embryos (generated by heterozygous cross) and maintained in cell culture for expression analysis after genotyping. By RT-PCR, we detected much less transcripts of Scyl1bp1 in mutant ("mutant" only refers to homozygous, the same for later) MEF than in heterozygous MEF (**Fig. 9a**). By RealTime PCR, the mRNA level in mutant MEF was quantified as 10% of WT level (**Fig. 9b**), which was supported by the result from the Western blot. As shown in

(**Fig. 9d**), Porostin protein was hardly detectable in mutant MEF, by contrast, abundant proteins were present in heterozygous MEF. The same result arose from immunofluorescence staining. Using the polyclonal Ab against Porostin, we detected typical Golgi-localized signal in heterozygous MEF (**Fig. 9c**). By contrast, such signal was not observed in mutant MEF (**Fig. 9c**), consistent with the result from RT-PCR and Western blot. Therefore, we conclude that high knock-down efficiency is achieved in our homozygous mice.

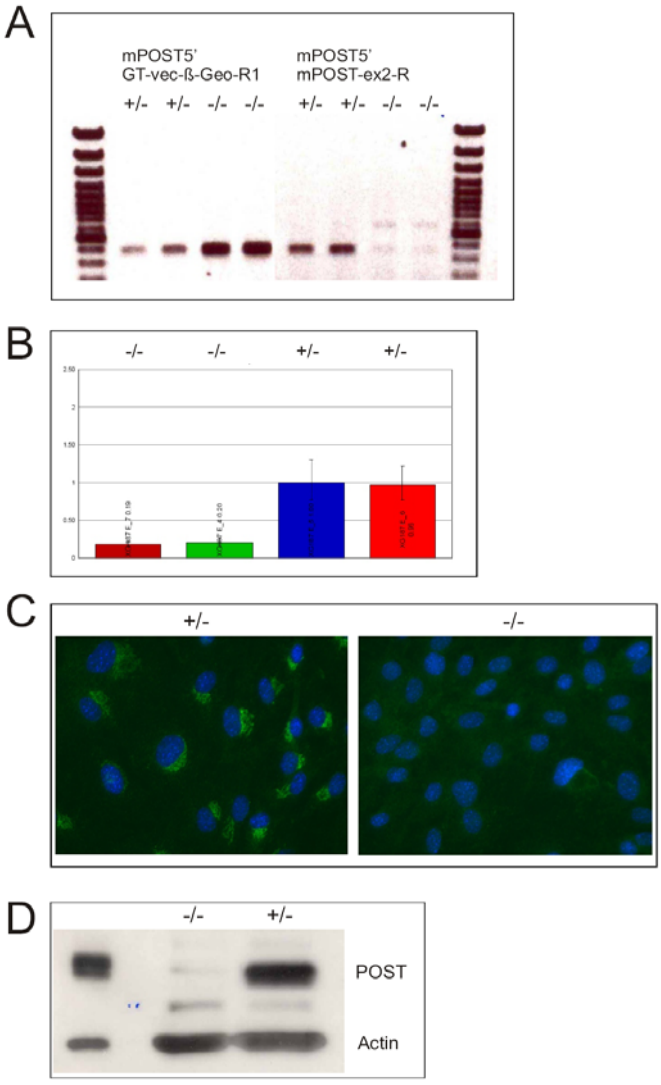


**Fig. 9.** Characterizing the expression of Scyl1bp1 in gene trap mouse. (A) Using RT-PCR, we detected little mRNA in homozygotes corresponding to the normal transcript (right side). Recombined mRNA between exon-1 of Scyl1bp1 and gene trap vector exon was detected in both heterozygous and homozygous cells, and homozygotes showed double amount of heterozygotes (left side). (B) By quantitative PCR, the normal Scyl1bp1 mRNA in homozygotes was normalized to less than 10% of WT level. (C) By immunofluorescence approach, the Porostin protein was hardly detectable in mutant MEF. (D) Western blot showed little expression of Porostin in homozygote compared with abundant amount in heterozygote. As a positive Ctl, overexpressed murine Porostin was on the left lane.

# 3.3 Phenotype of Scyl1bp1 deficient mice

## 3.3.1 Lethality phenotype

### 3.3.1.1 Lethality of homozygotes

After breeding with C57BL/6, the founder chimeras produced F1 progeny. By genotyping, some of the progeny produced by founder chimeras #1651, #1652, #1670 were identified to be heterozygous, demonstrating that these founder chimeras carry the mutant allele in germ-line cells. These heterozygotes were bred with C57BL/6 wild type to produce more heterozygotes, and to get a defined genetic background. Heterozygous matings did not result in any homozygous mutants at the time of wearing and the ratio between heterozygotes and WT (61:29 till Jan 30, 2008) indicated that the homozygous mutants are likely to be embryonic-lethal.

### 3.3.1.2 Identifying homozygotes at embryonic stages

To look for the homozygous progeny, we collected mice of different embryonic stages generated by heterozygous mating and could identify homozygous embryos at E12.5, E14.5, and E17.5.

As homozygous embryos could be identified as late as E17.5, we switched our focus to the prenatal stages and got homozygous embryos at E18.5. Genotyping of fetuses at E18.5 obtained from Caesarean section did not reveal statistically significant loss of homozygous individuals up to birth. Fortunately, in one litter, we observed some newborns suffering from respiratory distress, which were subsequently identified as homozygotes. Noticeably, if we had not removed these homozygous newborns from the cage, the mother would have soon eaten them. The same observation made in the other litter assure us that the homozygotes died owing to respiratory insufficiency, which might be an explanation for the neonatal lethality.

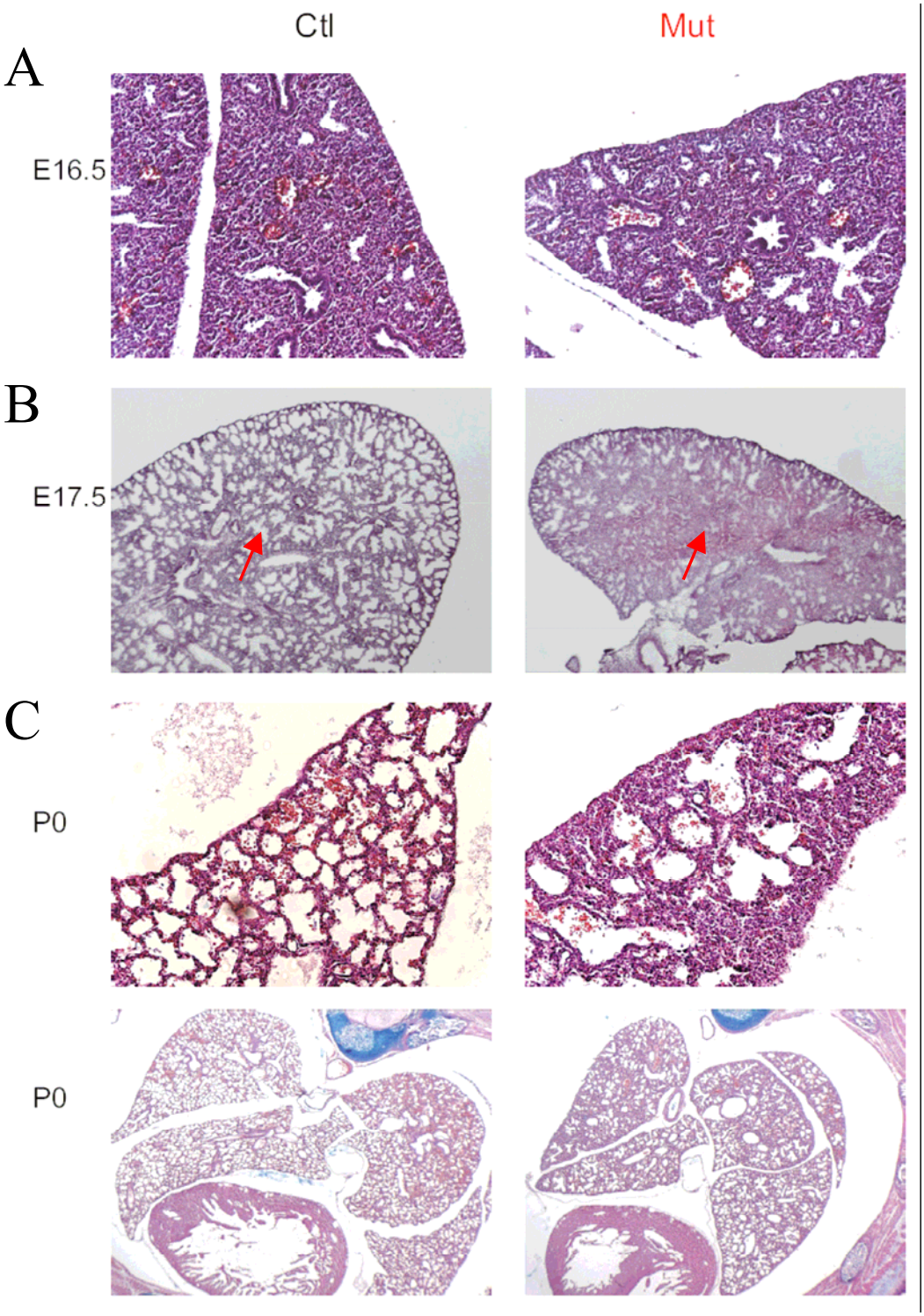


**Fig. 10.** Lungs of gene trap mice. (A) As late as E16.5, there was hardly any difference between mutant (homozygous) and Ctl lungs. (B) At stage of E17.5, the structure of lung was well formed in Ctl compared with mutant lung which was less differentiated, especially the inside part, indicated by arrow. (C) This difference accelerated at prenatal stage, when the mutant lung was less mature with thicker wall of alveoli compared with Ctl (upper panel). From a global view, mutant lungs have less air space compared with Ctl, however, the bulk of lungs is similar (lower panel).

### 3.3.1.3 Respiratory insufficiency in newborn homozygotes

The fact that the neonatal homozygotes died of respiratory distress shortly after birth turned our attention to the mutant lungs. The Haematoxylin & Eosin (HE) staining combined with Alcine Blue was applied to paraffin section of neonatal mouse lungs. As shown in (**Fig. 10c**), the homozygous lungs seemed to be less differentiated. In a global view, there is much less air space in the homozygous lung than in the Ctl. Moreover, the layer of alveolar sac was organized with multiple cells, compared with single cell layer in the Ctl (**Fig. 10c**).

To gain the view of lung structure by a developmental approach, we examined the lung development at E16.5, E17.5, and P0. As shown in (**Fig. 10a**), there was no difference between mutant and WT at E16.5. The significant difference emerged since E17.5, when the mutant lungs, especially the inside part, were less mature compared to Ctl (**Fig. 10 b**). The ill-distribution of some cells might give rise to some defect during alveolar formation in mutant lungs.

Interestingly, if we took out of E18.5 embryos by Caesarean section and cleared the airways (especially removing viscous liquid in the mouth ) before putting them in warm surroundings, the homozygous mutants could survive up to 3h (longer time not tested) even though they displayed a bit higher frequency of breathing than WT and heterozygotes. The lungs dissected from E18.5 mutants floating in 1×PBS also indicated that breathing had been successfully made in light of the lungs full of air.

### 3.3.1.4 Surfactant proteins in the mutant lungs

Whereas Nuclear factor I-B deficient mice died of respiratory failure, the heterozygotes did survive (Grunder et al., 2002). When compared with $Nfib^{+/-}$, our homozygous mutants exhibited even mild abnormality. Therefore, there might be something else that contributes to lethality.

Surfactant proteins in the air/liquid interface of the lung are essential factors to lower the surface tension for air entry. Especially, surfactant protein B (SP-B) was demonstrated to be the most crucial one (Clark et al., 1995). We therefore examined the expression of SP-B

and SP-C in lungs by immunohistochemistry approach and detected a bit less SP-B in mutant lungs, however, SP-C was unaffected compared with WT (**Fig. 11**).

We conclude that our mutant mice suffer from respiratory insufficiency, but still they could survive beyond 3 hours with some assistance (e.g. clear the airway and put them in warm surroundings). It is also possible that these mutants might overcome breathing defect completely if further measures (e.g. treatment with surfactant proteins) are taken.

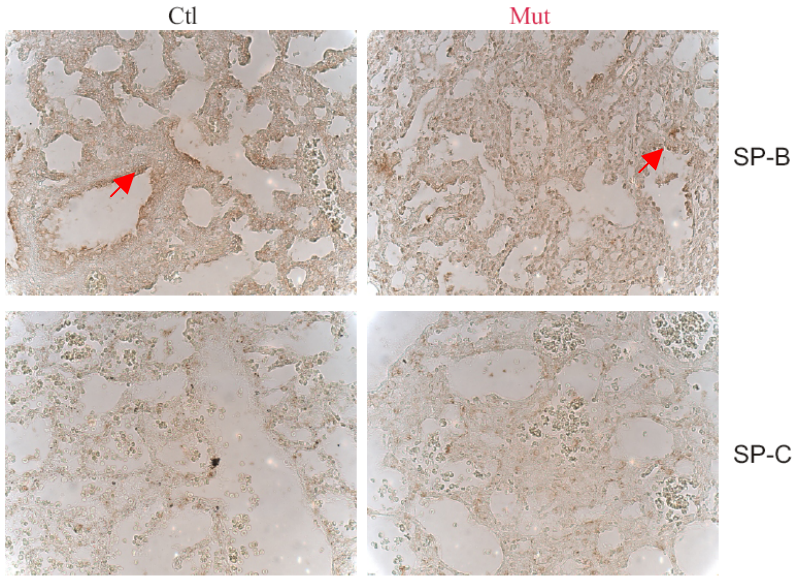


**Fig. 11.** Surfactant proteins in mouse lungs. Immunohistochemistry was performed using antibodies against SP-B and SP-C, respectively at P0. Less SP-B was detected in mutant lungs than in the Ctl, indicated by arrow (upper panel), however, no difference was observed for SP-C (lower panel).

### 3.3.2 Skin phenotype

Wrinkly skin, one characteristic symptom of GO, is already obvious in new born individuals with GO. Close observation of the skin of E18.5 embryos revealed different texture in the homozygotes while normal histological stain did not reflect such a difference (data not shown). It is obvious that the skin looks more redundant in the Ctl compared with the tightly stretched skin in the homozygotes (**Fig. 12**). We speculate that the tightly stretched skin in the homozygotes would slowly lose its elasticity with development and lead to wrinkly symptom in the later phases that however can not be investigated due to the postnatal lethality.

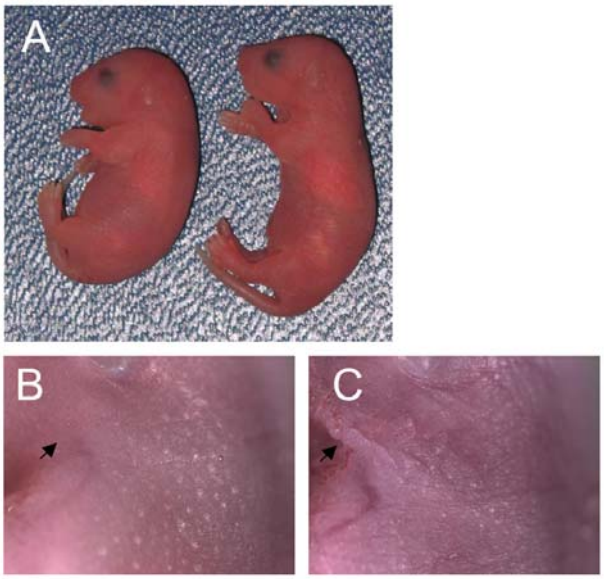


**Fig. 12** Skin phenotype of Scyl1bp1 deficient mice. (A) Image of E18.5 homozygous embryo (left) and Ctl (right) showed that homozygote is slightly shorter than Ctl and have bigger belly. (B-C) Close watching revealed tightly stretched mutant skin (B) compared with redundant Ctl skin (C), as indicated by arrow.

### 3.3.3 Bone phenotype

Osteoporosis is one obvious feature of GO patients. To figure out the role for Porostin in bone formation, we employed an in vitro assay termed "chicken bone marrow cells (chBM)" by overexpressing Porostin driven by RCAS retrovirus. In this system, we demonstrated a delay of differentiation in the cells infected by RCAS-POST, indicated by Alizarin red staining, compared with the cells infected by GFP or Ctl RCAS viruses ( **Fig. 13**). This might be due to partially impaired/disturbed function of Golgi apparatus in Porostin-overexpressing cells, which should also explain the osteoporosis in GO patients because loss of Porostin could similarly impair/disturb some aspects of Golgi function. Accordingly, the analysis of bone development in Scyl1bp1 deficient mice also revealed an ossification delay, as was demonstrated in the E18.5 Femur ( **Fig. 14b**). Importantly, the delay can be already observed in the primary ossification center at E14.5 ( **Fig. 14a**). In addition, we observed an ossification defect in the skull and a hypoplastic mandible reminiscent of the patient phenotype (**Fig. 14c,d**).

In conclusion, our mouse model recapitulates the phenotype of the individuals with GO syndrome even though respiratory distress was not reported in human patients. We

attribute the latter to species difference. However, it is not surprising in that depletion of Fibulin-4 or Fibulin-5 in mice also causes respiratory distress while mutations of them cause cutis laxa in humans (McLaughlin et al., 2006).

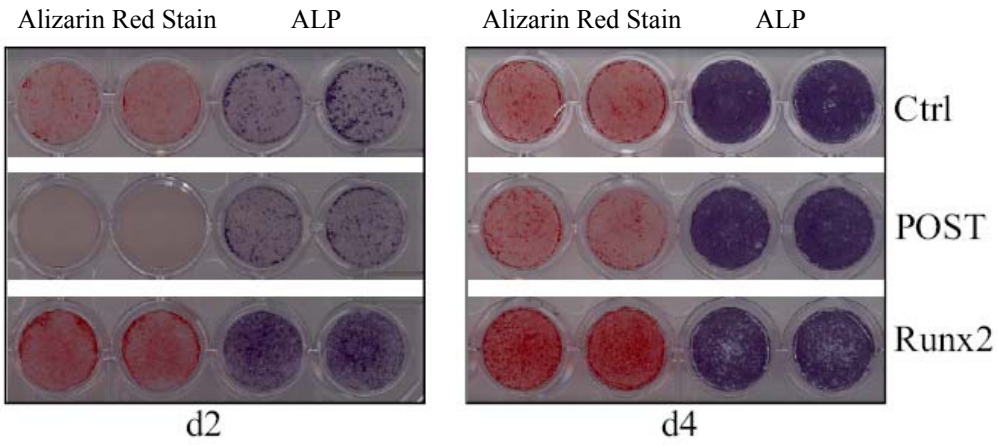


**Fig. 13.** Overexpression of Porostin caused mineralization delay in chBM. After switching into stimulation medium containing 10mM beta-Glycerophosphate and 50μg/ml Ascorbic acid, confluent chBM without virus infection or infected by GFP virus (Ctl) started mineralization in 2 days (upper of the left panel); chBM infected by Runx2 virus, as a positive Ctl, accelerated this process (lower of the left panel); chBM infected by Porostin virus slowed down the mineralization process, indicated by Alizarin red staining (middle of the left panel). However, alkaline phosphatase (ALP) activity was not affected by overexpression of Porostin.

## 3.4 Scyl1bp1 is ubiquitously expressed with higher level in lung, skin, cartilage and osteoblasts

### 3.4.1 *in situ* hybridization and RealTime PCR

To gain more functional information about this new member of Golgi resident proteins, we explored its expression level in different tissues. RealTime PCR result indicated the broad expression pattern of Scyl1bp1 in all the tissues tested, with relatively stronger expression in lung, skin and osteoblasts (**Fig. 15a**). By *in situ* hybridization in E14.5 mouse limb, we showed that Scyl1bp1 is expressed in nearly every cell type at low levels and confirmed higher expression in skin and cartilage (**Fig. 15b-f**).

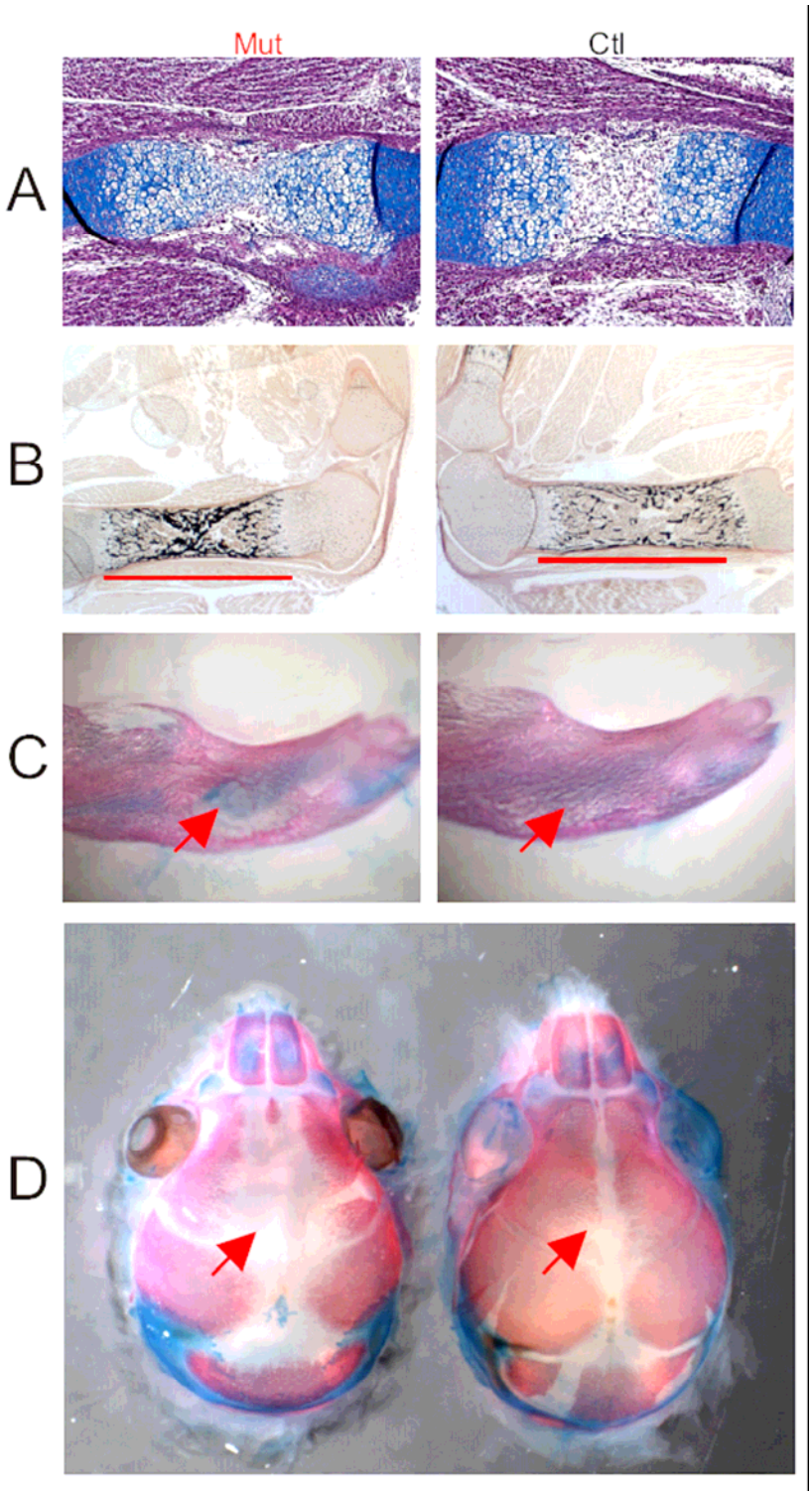


**Fig. 14.** Bone phenotype of Scyl1bp1 deficient mice. (A) Ossification delay was demonstrated in E14.5 humerus. (B) Ossification shortened in E18.5 femur, indicated by bar. (C) Ossification delay in E18.5 mandible bone, indicated by arrow. (D) Ossification delay in P0 skull, indicated by arrow.

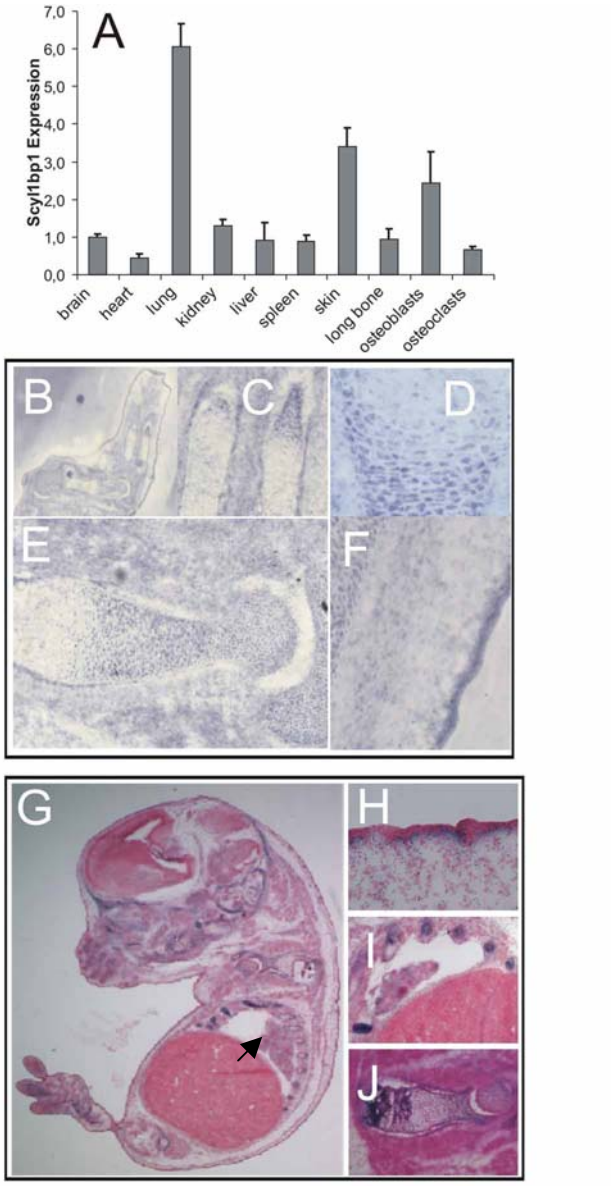


**Fig. 15.** Expression pattern of Scyl1bp1. (A) By real-time PCR, we detected Scyl1bp1 in all tissues tested, with stronger expression in lung, osteoblasts and skin. (B-F) By *in situ* hybridization with E14.5 mouse limb, we observed ubiquitous expression pattern, with higher level in cartilage (C,D,E) and skin (F). (G-J) By X-Gal staining with our gene trap mice, we could monitor the expression of Scyl1bp1 during embryonic development (E14.5). Higher expression level was observed in lung (G arrow), skin (H) and cartilage (I,J).

## 3.4.2 X-gal staining

Using the *Scyl1bp*$^{Gt(Bgeo)}$ mutant mouse line generated by insertion of a gene trap cassette into the first intron of the murine gene we were able to follow the Scyl1bp1 expression pattern during mouse development. X-gal staining confirmed its broad expression and also pointed out the higher expression in the bone and skin, representing the most affected organs in GO patients (**Fig. 15g-j**).

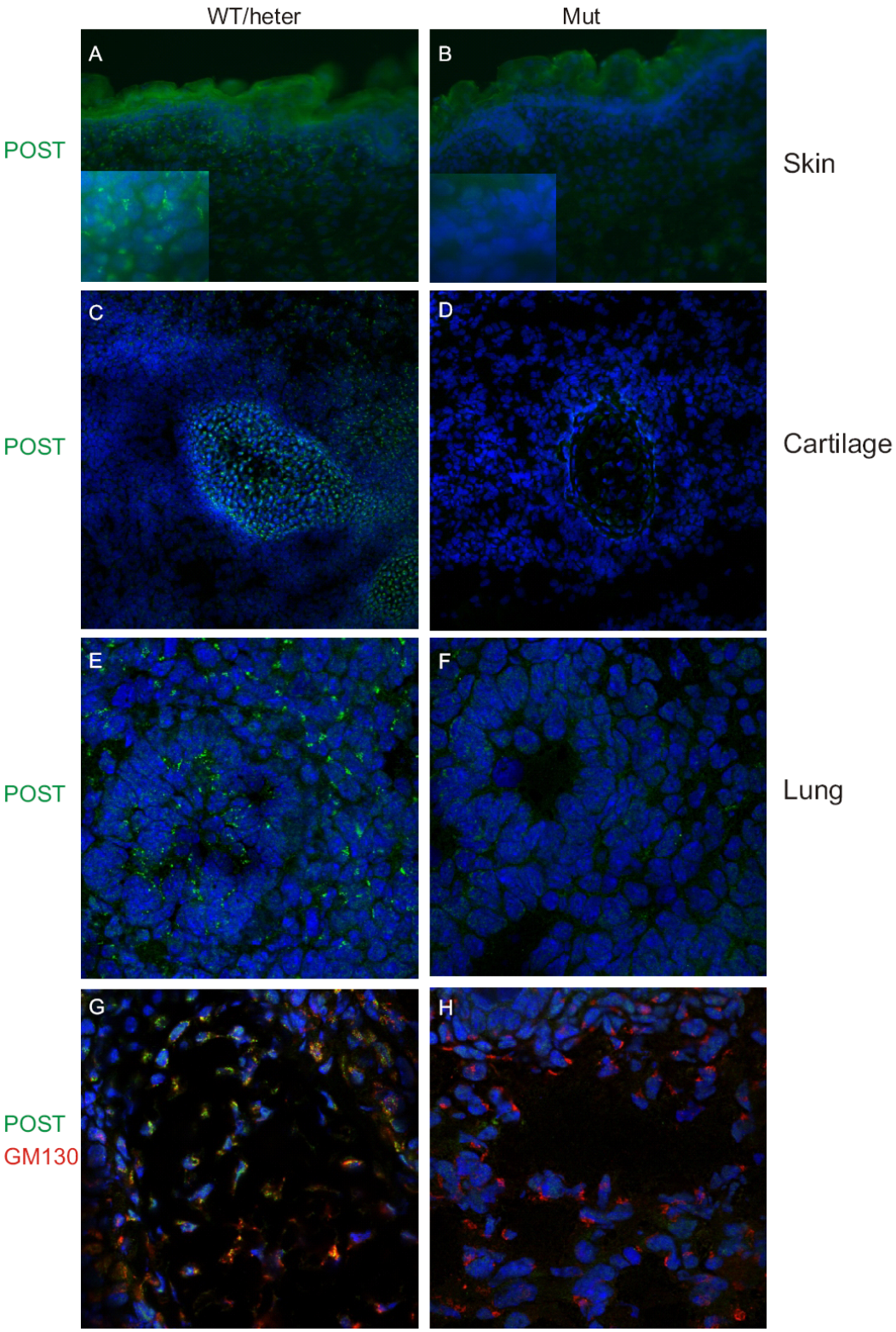


**Fig. 16.** Porostin immunostaining in mouse tissues. Polyclonal antibody against Porostin (POST; green) was used and the expression of Porostin was broad. (A) higher level was detected in the skin; (C) higher expression in cartilage; (E) higher expression in lung. (B,D,F) By contrast, little expression of Porostin was detected in mutant tissues. Double staining was performed for G&H ( green PolyPOST; red GM130). (G) Colocalized signal between Porostin and GM130 was observed in Ctl mouse tissues. (H) In comparison, only GM130 signal was detected in mutant tissues. DAPI was used for counterstaining.

### 3.4.3 Immunostaining

Immunostainings in the WT E14.5 whole embryo and E17.5 limb cryo-sections also revealed the broad expression pattern of Scyl1bp1 (**Fig. 16**). By co-staining with Golgi-marker GM130 antibody and anti-Porostin polyclonal antibody, we observed co-localization in every cell type investigated (**Fig. 16g**). By contrast, Scyl1bp1 was not detectable in the sections from *Scyl1bp1*$^{Gt(Bgeo)/Gt(Bgeo)}$ embryos (**Fig. 16b,d,f)**, in comparison with unchanged GM130 signal (**Fig. 16h**), which corroborated specificity of the anti-Porostin Ab (**Fig. 16a,c,e**). Consistent with *in situ* hybridization, RT-PCR and X-gal staining, the dermal layers of the skin (**Fig. 16a**), cartilaginous bones (**Fig. 16c**), as well as lung (**Fig. 16e**) demonstrated a higher expression level.

## 3.5 SCYL1BP1 specifically interacts with Rab6

Cells produce a large quantity of proteins that are transported to the plasma membrane or that are secreted. After receiving the newly synthesized proteins and lipids from rough endoplasmic reticulum, the Golgi apparatus undertakes a series of processing tasks such as modifying, sorting, and packaging. All these intricate processes are strictly and precisely regulated by different factors such as small G proteins within this organelle. As a Golgi resident protein with coiled-coil domains, SCYL1BP1 might play some role in the process of coordinating the transport and modification of continuously entering proteins. Depletion of SCYL1BP1 might therefore disturb this elaborate network, which in turn causes GO syndrome.

### 3.5.1 Y2H screen

Small G-proteins, a group of monomeric intracellular proteins with GTP/GDP binding and GTPase activities, are important regulatory elements that control a wide variety of cellular processes including cell growth/differentiation, cytoskeletal configuration, and intracellular vesicle transport. The switch between GTP-bound and GDP-bound states is controlled by guanine nucleotide exchange factors (GEFs), which trigger the binding of GTP and GTPase-activating proteins (GAPs), which accelerate hydrolysis of the bound GTP to GDP (Bos et al., 2007). In their GTP-bound form, Arf and Rab family GTPases associate with distinct organelle membranes, to which they recruit specific sets of effector proteins that regulate vesicular transport (Kawasaki et al., 2005). A variety of different effectors can

interact with one small G protein and translate the signal to several aspects of membrane transport, therefore contributing to the specificity in membrane trafficking (Grosshans et al., 2006).

Several Golgi proteins with coiled-coil domains have been reported to associate with members of the Rab family of small GTPases in membrane trafficking. Since SCYL1BP1 is a soluble protein with a coiled-coil region, we performed a yeast-two-hybrid screening for interaction partners from a library containing small G-proteins of the Arl, Arf and Rab families in collaboration with Dr. Francis A. Barr.

#### 3.5.1.1 Y2H constructs

SCYL1BP1 is a conserved protein with 74.8% amino-acid (aa) identity between mouse and human (**Fig. 17a**). Since there is one DFU662 domain with unknown function (179aa) covering two coiled-coil domains, we constructed different versions either including or excluding this region for the Y2H screen. Full length SCYL1BP1 was called "version 1"; the N-terminal part just including DFU662 domain was called "version 2"; the DFU662 domain alone was called "version 3" and the C-terminal part adjacent to DFU662 was called "version 4" (**Fig. 17b**).

To clone all the versions of SCYL1BP1 into pACT4-1b (lexA) and pBTM117c (bait) with $Amp^+$, kind gifts from Dr. Erich Wanker (MDC Berlin), we generated PCR products with SalI & NotI recognition sites on 5'- and 3'- ends, respectively. Because there is a SalI recognition site in the gene, we point mutated T→C (agt→agc, Ser) to block this site without aa exchange. After digesting these PCR products as well as Y2H vectors pACT4-1b and pBTM117c with SalI & NotI, ligation was performed with purified products. To insert full length of SCYL1BP1 into pFBT9 (Bait) with $Kan^+$, kindly provided by Dr. Francis A. Barr, ligation was performed between BclI & SalI double digested PCR product and BamH I& SalI double digested pFBT9 plasmid.

All the constructs were confirmed by sequencing before Y2H screening in a small G protein library. Y2H screening was performed by the Group of Dr. Francis A. Barr at Max Planck Institute for Biochemistry, Martinsried.

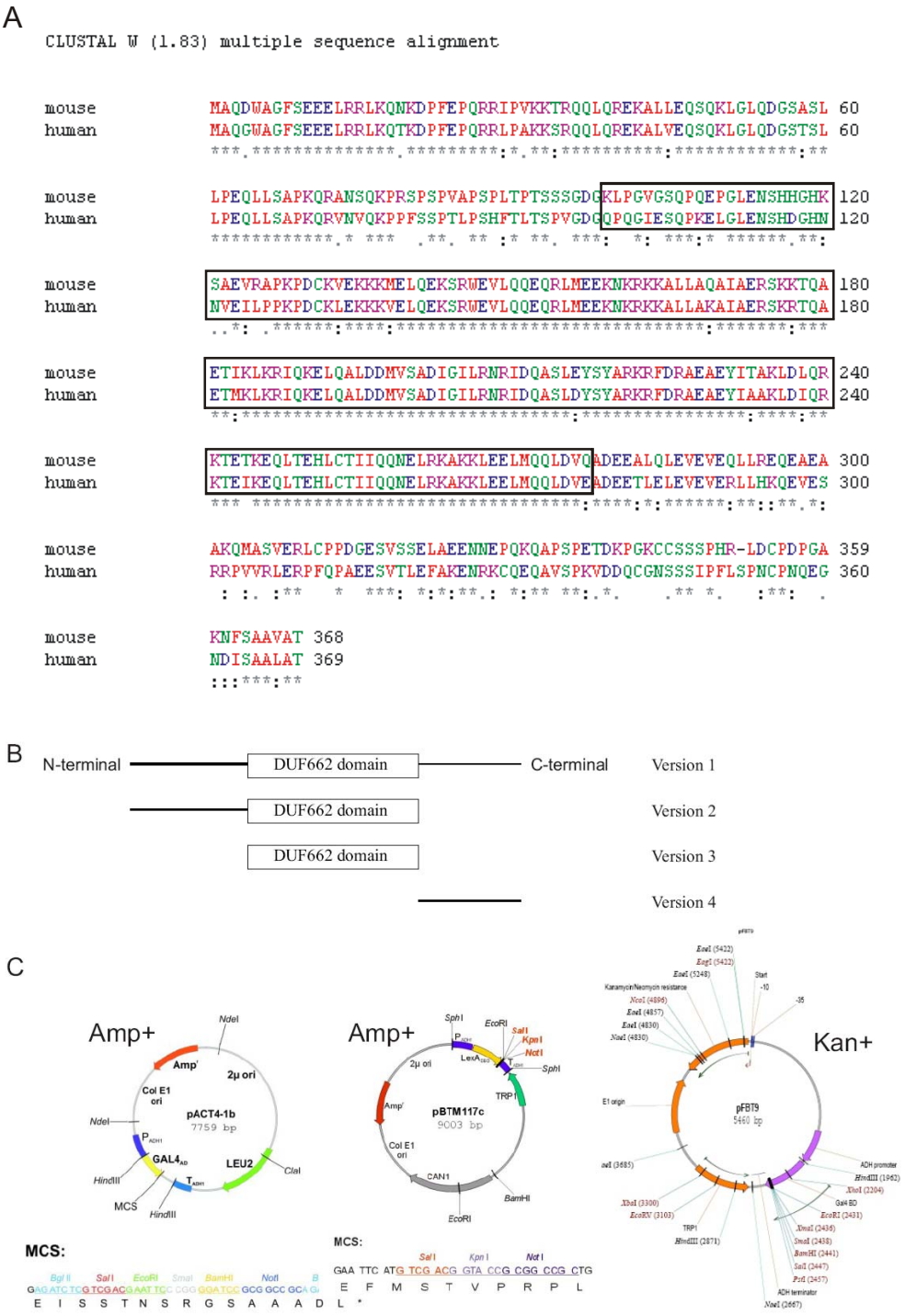


**Fig. 17.** Y2H screening construction. (A) DFU662 (in a frame), one domain with unknown function, was highly conserved between mouse and human. (B) Different versions either including or excluding this domain were constructed for specific interaction test. (C) The vectors used in this study included pACT-1b, pBTM17c and pFBT9. The maps of these vectors were shown.

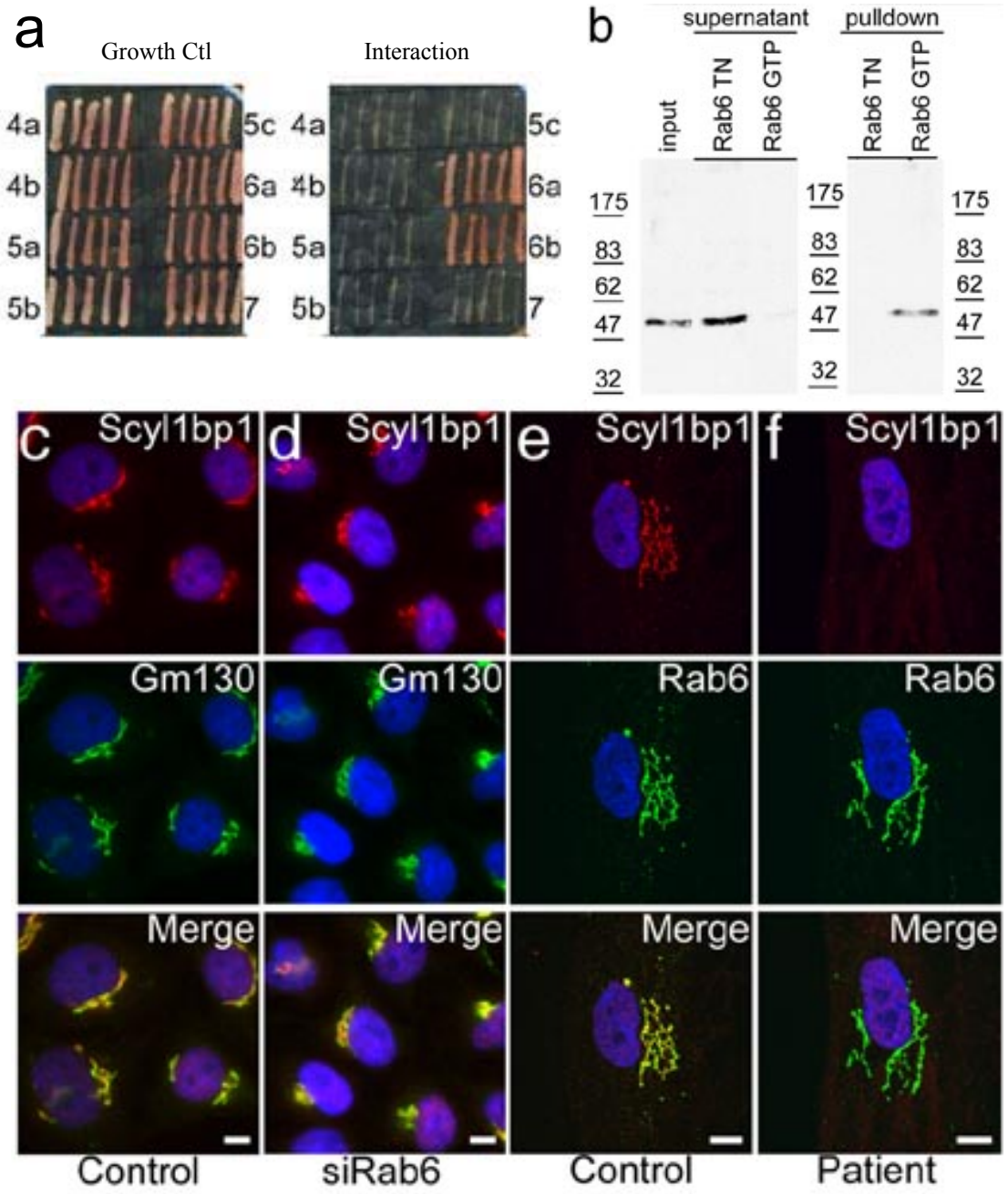
a
Growth Ctl
Interaction
4a
4b
5a
5b
5c
6a
6b
7
b
supernatant
pulldown
input
Rab6 TN
Rab6 GTP
175
83
62
47
32
c
d
e
f
Scyl1bp1
Gm130
Rab6
Merge
Control
siRab6
Control
Patient
g
Rab6 QA
POST
Full Length
PCR4
PCR6
PCR8
N
C
Rab6 TN
Interaction
Growth Ctl

Fig. 18 SCYL1BP1 specifically interacts with Rab6. (a) Results of a yeast-two-hybrid screening for interaction of SCYL1BP1 with the Rab family of small GTPases showing specific interaction with Rab6a and Rab6b. The left panel shows the growth control, the right panel shows the results of the interaction screening. (b) Confirmation of the Rab6 interaction by pulldown experiments. A GST-Rab6 fusion protein was used to pull down SCYL1BP1 from HeLa lysates without or in the presence of GTP. GTP-bound Rab6 pulled down SCYL1BP1 so efficiently that only small amounts remain detectable in the supernatant. (c) Co-localization of SCYL1BP1 with GM130 in HeLa cells. (d) Co-localization of SCYL1BP1 with GM130 after treatment with a Rab6 siRNA. No significant change in the subcellular localization was evident. (e) Co-localization of SCYL1BP1 with Rab6 shows highly overlapping signals. (f) In GO patient cells deficient for SCYL1BP1 subcellular distribution of Rab6 seems not altered. (g) Coiled-coil domains are sufficient for the interaction. By Y2H, deletion mutants of SCYL1BP1 revealed that the interaction is mediated by the SCYL1BP1 coiled-coil domains. Furthermore, SCYL1BP1 interacts specifically with Rab6-GTP (Rab6 QA), but not with Rab6-GDP (Rab6 TN). Scale bar = 10 μm.

#### 3.5.1.2 Binding partners

With full length SCYL1BP1 (version 1), a specific interaction between SCYL1BP1 and Rab6 was identified (**Fig. 18a**). The different deletion versions were subsequently used to map the region mediating the interaction with Rab6. By Y2H, the versions 1, 2 and 3 had similar binding ability to Rab6, by contrast, version 4 lost its affinity, indicative of the sufficiency of coiled-coil domains for this interaction (**Fig. 18g**). Pulldown experiments further demonstrated that SCYL1BP1 specifically interacts with the GTP-bound active form of Rab6, while Rab6 TN, the inactive form failed to bind (**Fig. 18b**).

Rab6 is a central player in membrane trafficking. Rab6 participates in the retrograde transport from endosomes to the Golgi as well as the membrane trafficking in the secretory pathway, therefore both of them might contribute to the GO pathogenesis.

#### 3.5.1.3 SiRNA against Scyl1bp1

To address the role of SCYL1BP1 in the Golgi, we ordered 4 different siRNA duplexes against human Scyl1bp1 from QIAGEN. By testing different oligos, concentrations, and transfection reagents as well as cell lines, we demonstrated the high efficiency of oligo #1 in Hela cells 48h after transfection with INTERFERin from Polyplus-transfection (**Fig. 19**).

By specific siRNA against Scyl1bp1 or Rab6, we achieved efficient knock-down (~90%) in Hela cells, as was indicated by Western blot in comparison with control siRNA(**Fig. 19**). Surprisingly, deletion of Rab6 did not cause re-distribution of SCYL1BP1, and vice versa (**Fig. 18c-f**). This indicated that Rab6 is not prerequisite for the residence of SCYL1BP1 in the Golgi.

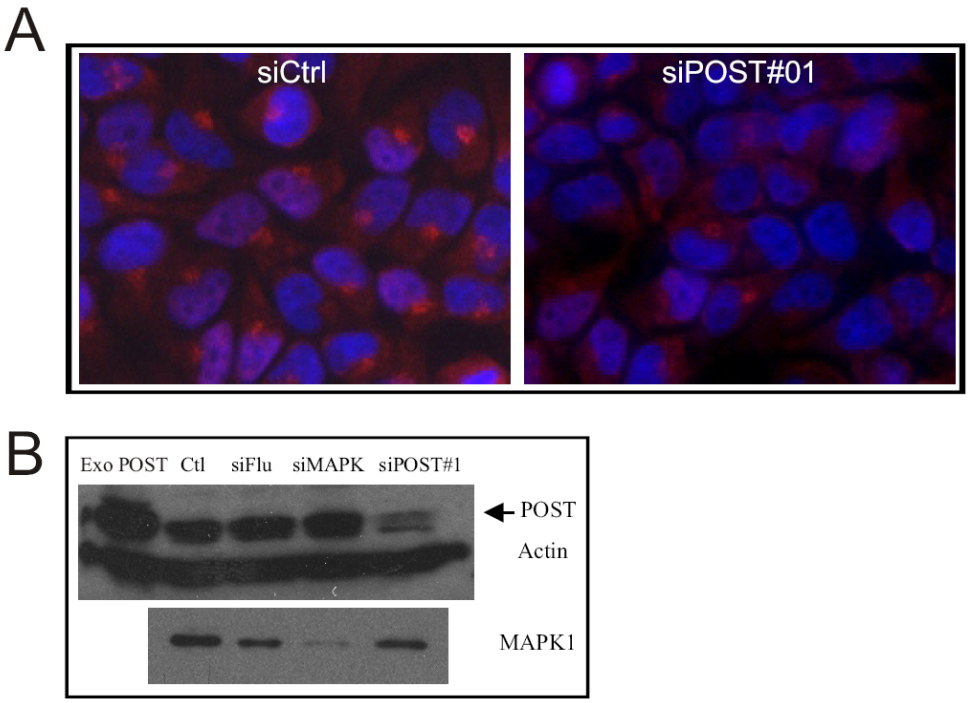


**Fig. 19.** Knockdown effect of siRNA #1 against Scyl1bp1. (A) Immunofluorescence with polyclonal antibody against Porostin showed high efficiency of knock down. 5 nM siRNA against MAPK1 and Scyl1bp1 (with random sequence siRNA as Ctl) was delivered into Hela cells with 8 µl PolyPlus INTERFERin reagent 12 h after seeding the cells in 6-well plate. To get sufficient knockdown effect, repeated transfection was made in 24 hours. (B) Western blot indicated that more than 80% of Porostin was depleted in #1 siRNA transfected cells compared with Ctl 60-72 h after the initial transfection. As a positive Ctl for Western blot, overexpressed Porostin (Exo POST) was loaded on the left lane. Polyclonal antibody against Porostin was used in the experiment and antibodies against Actin and MAPK1 were used as a loading Ctl and siRNA positive Ctl, respectively.

### 3.5.2 Secretion of proteins involved in elastogenesis

The specific interaction between SCYL1BP1 and Rab6 indicated that loss of Scyl1bp1 might affect some aspect of intracellular trafficking, leading to impairment of the exocytosis and secretion. For this purpose, we investigated the secretion of proteins relevant for elastogenesis by patient fibroblasts.

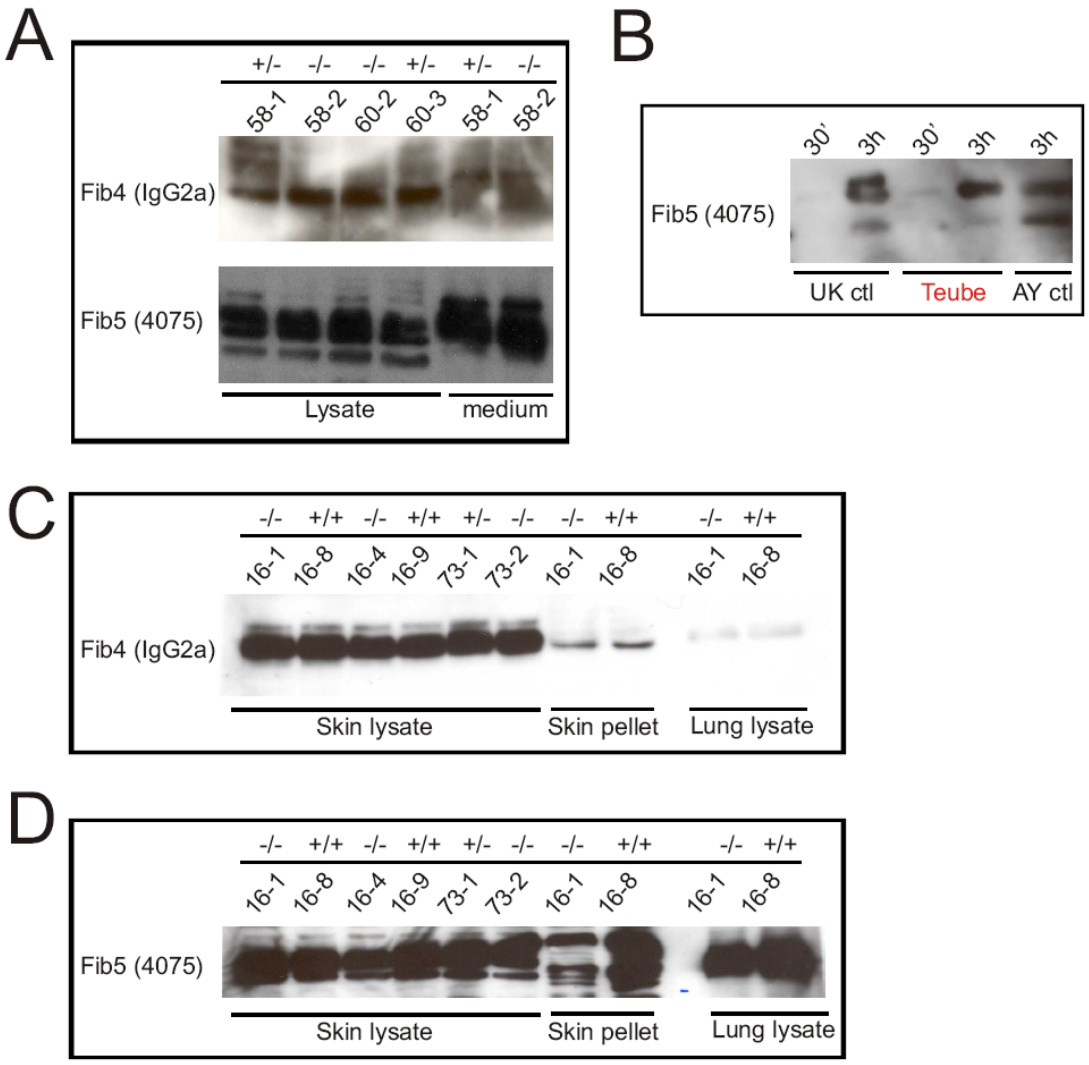


**Fig. 20.** Investigation of Fibulin-4&5 in the in vitro and in vivo systems. (A) With MEF cells derived from our gene trap mice, we studied the content of Fibulin (Fib)-4&5 in cell lysates and medium. We did not observe reduced expression or secretion of Fib4&5 in mutant cells. (B) To monitor the minor difference likely existing in secretion rate, we starved cells overnight followed by culturing them in complete medium. As short as 30 min after feeding cells with complete medium, Fib5 secreted into medium was detectable. 3 hours after changing medium, similar abundance of Fib5 was present in the medium from both Ctl and patient (Teube) HAF cells. (C-D) By taking advantage of gene trap mice, we analyzed the expression of Fib4&5 in the skin and lungs. Similar expression level was detected in the lysates from mutant and ctl tissues. However, in the skin ECM (pellet), a bit less Fib5 was detected in mutant compared with ctl (D).

Fibulin-5 and Fibulin-4 have been recently identified to be components of extracellular elastic fibres. Mutations in both cause cutis laxa in humans (Hucthagowder et al., 2006; Loeys et al., 2002; Markova et al., 2003). In addition, ablation of Fibulin-5 or Fibulin-4 in

the mouse caused lung abnormality and the latter died shortly after birth (McLaughlin et al., 2006; Nakamura et al., 2002). All these phenotypes resemble the pathological changes in Scyl1bp1 deficient mice. Therefore, Fibulin-4 and Fibulin-5 are good candidates that might be involved in GO pathogenesis.

To compare the amount of Fibulin-4 and Fibulin-5 in the medium from mutant and Ctl cells, we cultured two lines of mouse MEF ( one from homozygous and the other from Ctl) in low serum medium for 24 hours. However, no reduction was observed for mutant cells (**Fig. 20a**), and the same result came from the comparison between human patient HAF and Ctls. A similar amount of Fibulin-4 and Fibulin-5 was also detected in mutant and Ctl cell lysates (**Fig. 20a**). To look for the minor difference which might exist between WT and mutant, we monitored the dynamic secretion of Fibulin-5 after washing the cells with PBS prior to incubation with low serum medium. 30 min after incubation, we already detected some Fibulin-5 in the medium collected from patient HAF, however, it was hardly detected in Ctl medium(**Fig. 20b**). At 3h, similar amounts of Fibulin-5 were detected in patient and ctl medium (**Fig. 20b**). These data indicated no significant delay for Fibulin-5 secretion in patient fibroblasts. Moreover, Fibulin-4 and Fibulin-5 fibril deposition by patient and Ctl fibroblasts several days after culture was similar (data not shown).

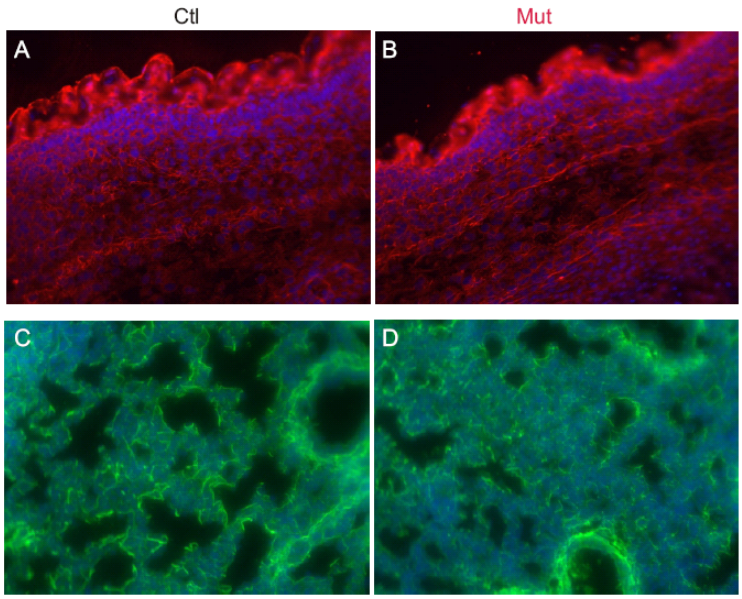


**Fig. 21.** Elastin immunostaining in mouse skin and lungs. (A-B) Elastin fibres in E17.5 limb skin were visualized by elastin antibody (RA75), which gave similar pattern in both Ctl and mutant samples. (C-D) Elastin fibres in E17.5 lungs. The amount of Elastin fibres in Ctl and mutant was similar. No other obvious abnormality was observed.

To test the difference of extracellular matrix which might exist in vivo, we compared the expression of Fibulin-4 and Fibulin-5 in mutant skin and lungs with the expression in Ctl tissues by Western blot. Similar amounts of proteins were detected either in extracellular matrix (ECM) or in soluble fractions from both tissues (**Fig. 20c,d**). A mild difference between Fibulin-5 ECM lysate needs further investigation. Moreover, we could not detect visible alterations of elastin fibres in the mutant skin and lungs (**Fig. 21**).

In summary, secretion of Fibulin-4 and Fibulin-5 was not obviously impaired in patient fibroblasts.. Moreover, Fibulin-4, Fibulin-5 and elasin fibres in the tissues of skin and lungs from mutant mice were not strongly affected by the loss of Scyl1bp1.

## 3.6 Glycosylation defect

Proteins destined for secretion are core glycosylated, folded, and assembled into oligomeric structures in the endoplasmic reticulum (ER). After moving to the Golgi complex, proteins are further modified by glycosyltransferases prior to their export to either the cell surface or the endocytic compartment. The Golgi complex provides well-ordered compartmentalization of oligosaccharide modification reactions that might otherwise compete (Pfeffer, 2007). Congenital disorders of glycosylation (CDG), also known as carbohydrate deficient glycoprotein syndromes, refer to a group of diseases in which oligosaccharide modifying processes are impaired (Jaeken and Matthijs, 2007).

Using a panel of lectins, we detected a highly reduced E-PHA signal in *Scyl1bp1*$^{Gt(Bgeo)/Gt(Bgeo)}$ skin samples both by histochemisty and Western blot (**Fig. 22**), indicative of a complex N-glycan processing defect. By Maldi-Tof, we confirmed the global defect of N-Glycans in *Scyl1bp1*$^{Gt(Bgeo)/Gt(Bgeo)}$ skin samples (**Fig. 23**), however, such a defect was not observed in *Scyl1bp1*$^{Gt(Bgeo)/Gt(Bgeo)}$ liver, lungs, or the whole embryo (**Fig. 24a**), which suggested that loss of Scyl1bp1 impaired glycosylaion specifically in the skin. This fits very well to the GO phenotype, in which skin is mostly affected without involvement of serum glycoproteins produced by the liver. Interestingly, when we tested the lysates from the MEF and HAF in culture, which were derived form the skin of mutant mice and GO patients, respectively, no obvious difference was observed compared to normal Ctls (**Fig. 24b**). This might reflect different conditions between in vitro and in vivo.

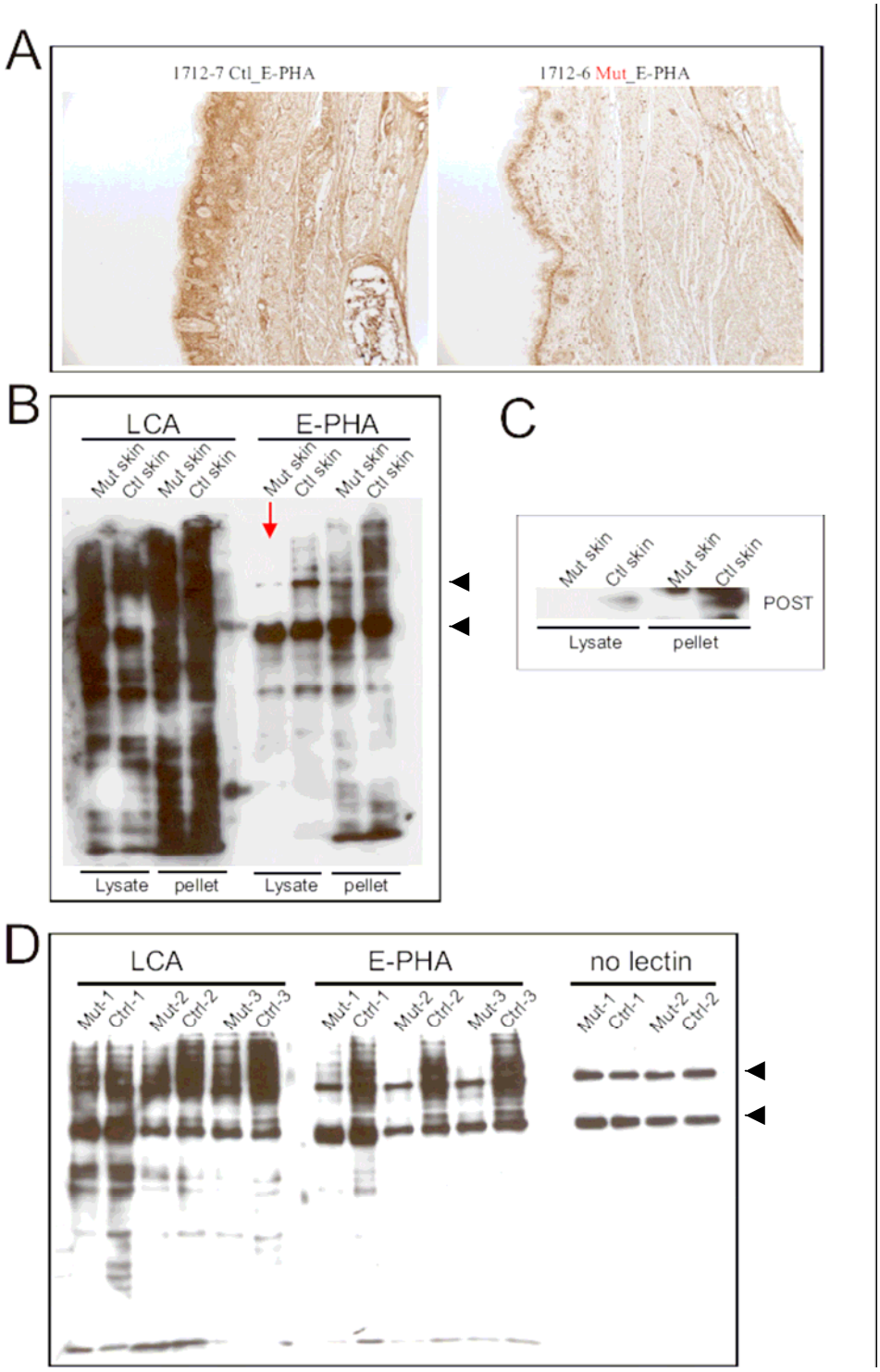


**Fig. 22.** Lectin histochemistry and blot of mouse skin. (A) E-PHA, a lectin recognizing complex N-glycans, gave weak signal in mutant skin (new born mouse) compared to Ctl skin. (B) By lectin blot, we showed that mutant skin was much less recognized by E-PHA compared to Ctl (indicated by arrow), by contrast, such a difference was not observed for LCA, a lectin recognizing high-mannose-type N-glycans. (C) The identity of mutant and Ctl skin samples was confirmed by Western blot. (D) Three pairs of mutant and Ctl skin samples showed consistent result. Note: two strong bands in all the blots, indicated by arrow head, should be regarded as background because they also appeared in the blot without any lectin.

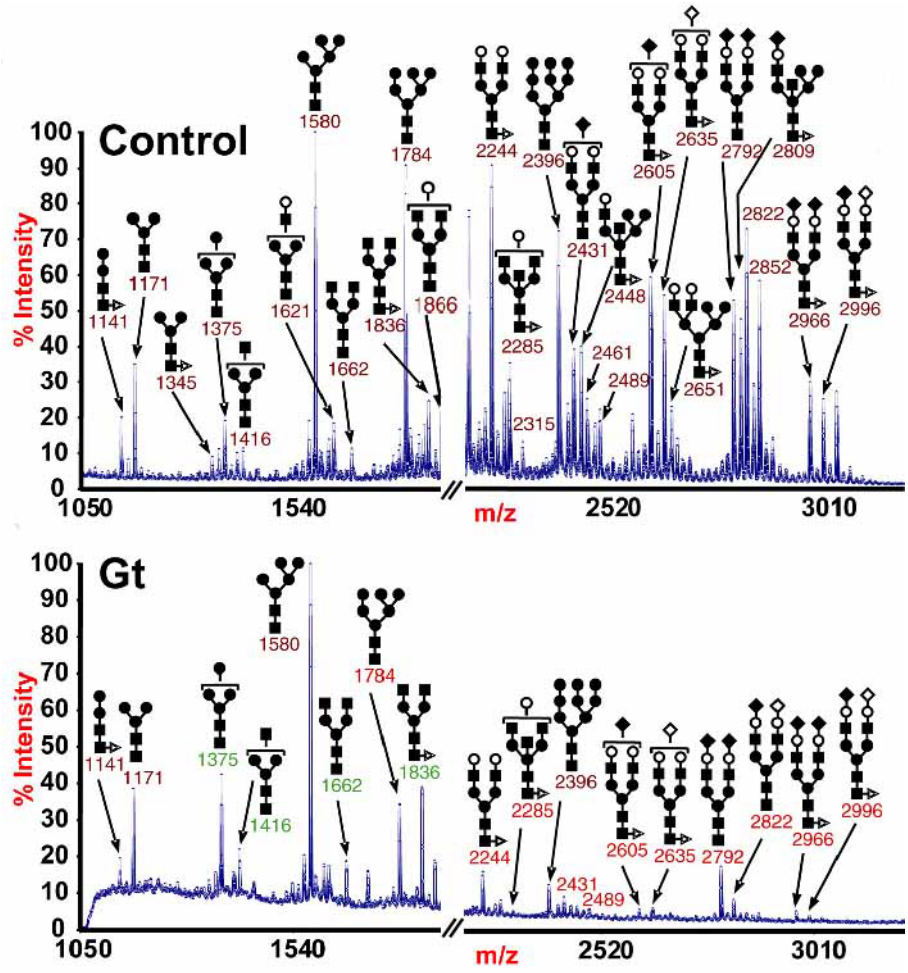


**Fig. 23** Maldi-Tof MS analysis of skin tissues. Mass spectrometric analysis of N-glycans from *Scyl1bp1*$^{Gt(Bgeo)/Gt(Bgeo)}$ mutant skin. *Scyl1bp1*$^{Gt(Bgeo)/Gt(Bgeo)}$ skin reveals a striking paucity especially of complex N-glycans, while some high mannose and hybrid N-glycans increase in abundance. Gt= *Scyl1bp1*$^{Gt(Bgeo)/Gt(Bgeo)}$ gene trap mutant. Ctl= wildtype or heterozygous controls. Red numbers= Glycan reduced in mutant, green numbers= glycan increased in mutant. ■ = N-acetyl glucosamine, ● = mannose, Δ = fucose, o = galactose, ◆ = sialic acid.

Since osteoporosis is the other feature of GO syndrome, we performed E-PHA staining on bone sections and revealed reduced E-PHA signal in the perichondrium of the Scyl1bp1 deficient mice (**Fig. 25**). We therefore conclude that loss of Scyl1bp1 leads to a glycosylation defect specifically in the skin and perichondrium, which might explain why GO patients suffer from wrinkly skin and osteoporosis, while other organs are unaltered despite the broad expression of this gene.

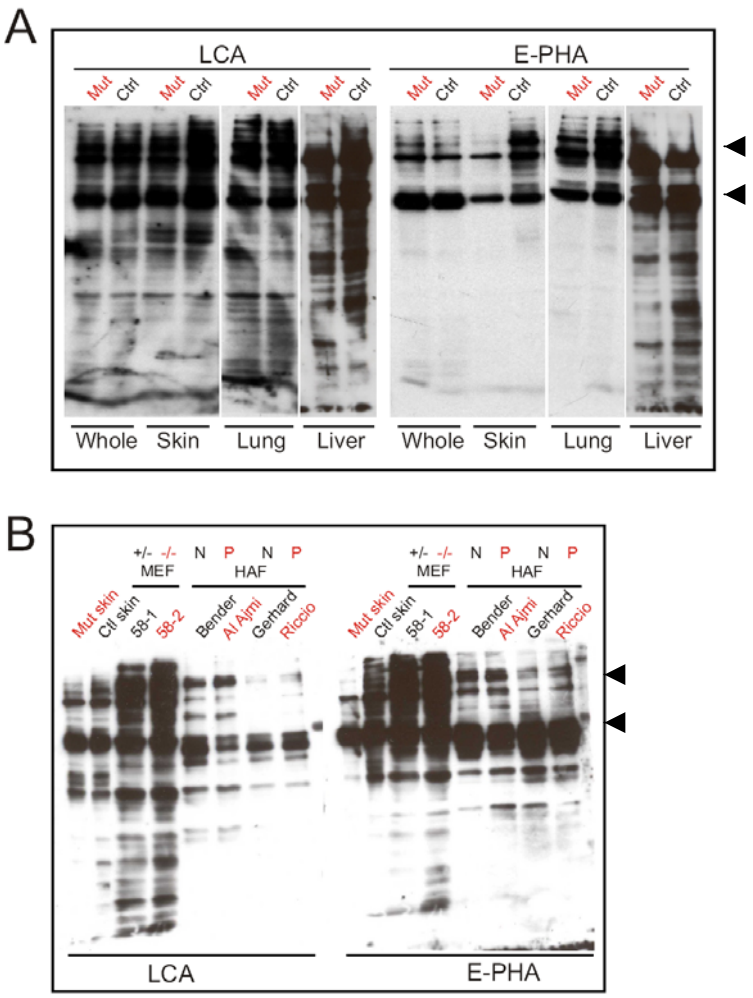


**Fig. 24.** Lectin blot of mouse tissues and cell lines. (A) Different mouse tissues including whole embryo (whole), skin, lung and liver were tested by lectin blot. There was no difference for LCA between mutant and Ctl for all the tissues (left side); E-PHA showed similar patterns between mutant and Ctl tissues except a difference in the skin (right side). (B) We tested MEF cell lysates (cell lines derived from gene trap mice) and HAF cell lysates (cell lines derived from GO patients and normal Ctls) by lectin blot, and no obvious difference was observed either for LCA or E-PHA between mutant and Ctl. Skin tissue lysates from mutant and Ctl mice were used as a Ctl.

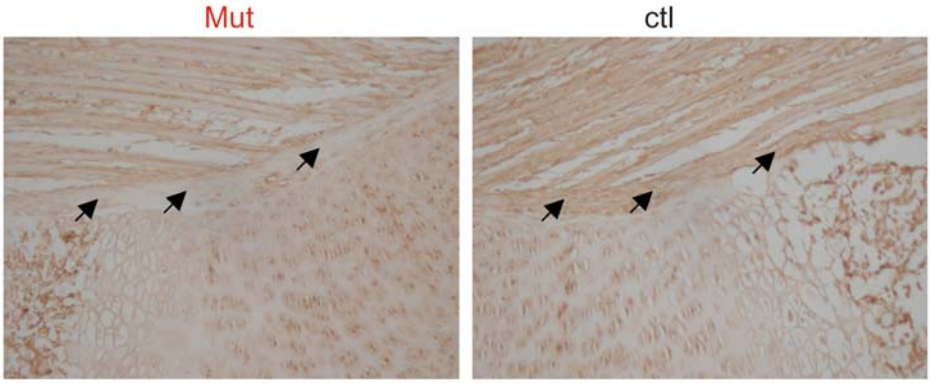


**Fig. 25.** E-PHA stain in E17.5 femur. E-PHA stain in the proximal femur revealed a reduced signal in perichondrium of the Scyl1bp1 deficient mice compared with Ctl (indicated by arrow).

## 3.7 Chip data analysis

As an independent section, however, in part serving the GO project, we took mouse embryonic forelimbs at different developmental stages (E11.5, E12.5, and E14.5) that reflect the progressive development of cartilage, and performed genome-scale screening for differentially expressed genes by Affymetrix gene chip. Special interest was shown in novel secreted factors that were up-regulated during this process (**Table 2**).

By performing section and whole mount *in situ* hybridization, we gained expression profile of a list of candidates, and showed great interest in the genes that were strongly/exclusively expressed in cartilage/ joint (**Fig. 26**). We cloned the full ORF of these genes into RCAS retrovirus vector and performed functional screening in chicken Micromass (chMM) and chBM in vitro systems by overexpression. A novel secreted factor, MSP05, displayed a mild induction of bone mineralization in chBM (**Fig. 27c**).

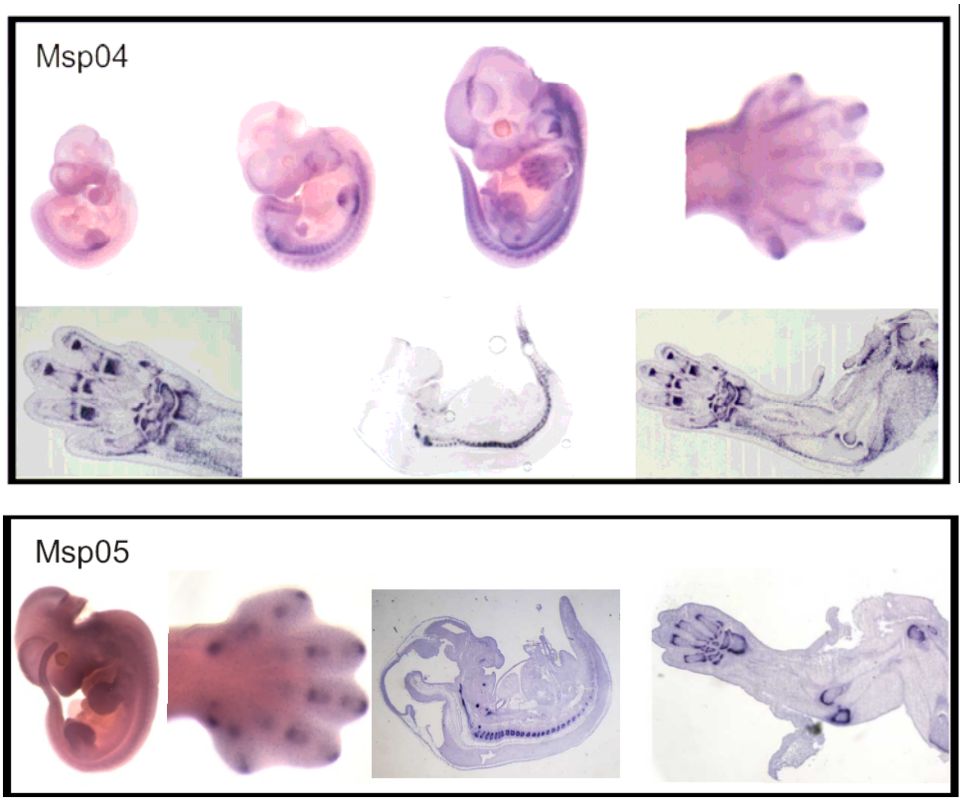


**Fig. 26.** *in situ* hybridization of two secreted proteins. Whole mount *in situ* was performed with E10.5, E11.5, E12.5 whole embryos and E13.5 limb for Msp04, E11.5 whole embryo and E13.5 limb for Msp05. Section *in situ* was performed with E12.5 embryo and E14.5 limb cryo-sections. Both Msp04 and Msp05 show strong expression in cartilage (especially around the joints).

| Our No. | Accession No. | Affymetrix ID | D11_Sig | D12_Sig | D14_Sig | Brief Description |
|---|---|---|---|---|---|---|
| MSP01 | XP_129714 | 1456335_at | 69,6 | 93,9 | 417,8 | secreted, Thrombospondin type I repeat; Somatomedin B (SMB) domain; human homologue present but function unknown |
| MSP02 | XM_131451.2 | 1430313_at | 20,3 | 45,7 | 157,6 | secreted, Thrombospondin type I repeat, function unknown |
| MSP03 | NM_029614 | 1431057_a_at | 6,9 | 25,5 | 70 | secreted, chymotrypsin activity; proteolysis and peptidolysis; function unknown |
| MSP04 | NM_026271 | 1419376_at | 53,3 | 132,8 | 176 | secreted, function unknown |
| MSP05 | XM_132070 | 1456793_at | 5,4 | 131,5 | 483,6 | secreted, Cytokine-like protein C17 precursor; function unknown |
| MSP06 | NM_011348 | 1442226_at | 24,7 | 84,1 | 207,3 | secreted; some role in neuroscience (outgrowing axons) |
| MSP07 | NM_024283 | 1460049_s_at | 2,1 | 1,3 | 144,2 | secreted, esophageal cancer related gene 4 protein, function unknown |
| MSP08 | NM_022315 | 1431362_a_at | 4,1 | 32,9 | 68,6 | secreted, modular calcium-binding protein 2, a novel angiogenic factor |
| MSP09 | NM_009136.1 | 1420764_at | 1,3 | 10,3 | 25,5 | secreted, some role in neuroscience |
| MSP10 | NM_028333. | 1421421_at | 1,5 | 3,4 | 45,9 | secreted, known function in angiogenesis, cardiovascular development |
| MSP11 | NM_175012 | 1424525_at | 1 | 6,5 | 42,1 | secreted, known function in memory and gastrointestinal tract |
| MSP12 | U25633.1 | 1416529_at | 129,4 | 275,1 | 712,7 | secreted, involved in cell growth and c-myc-induced tumor |
| MSP13 | BC006640.1 | 1448823_at | 39 | 57,8 | 353,3 | secreted, have an important role in development |
| MSP14 | BB810080 | 1437466_at | 227,4 | 418,8 | 1488 | secreted, activated leukocyte cell adhesion molecule, Perichondrium Express, Participate in Bone Marrow Formation |
| MSP15 | NM_008987.1 | 1418666_at | 26,5 | 40 | 112,6 | secreted, pentaxin related gene |
| MSP16 | NM_030127.1 | 1419292_at | 1,7 | 4,5 | 75,3 | secreted, HtrA3; important role in the formation/function of the placenta, regulation of cell growth, proteolysis and peptidolysis |
| MSP17 | BC006604.1 | 1424214_at | 5,6 | 14,1 | 87,2 | secreted, function unknown, rat homologue 70% castration induced prostatic apoptosis-related |
| MSP18 | BB499147 | 1453148_at | 38,4 | 97,5 | 145,8 | secreted, sema domain, immunoglobulin domain (Ig), short basic domain, (semaphorin) 3D |
| MSP19 | BC025654.1 | 1423915_at | 73,9 | 122,4 | 220,6 | secreted, olfactomedin-like 2B, function unkown |
| MSP20 | NM_021281.1 | 1448591_at | 29,1 | 54,7 | 174 | secreted, cysteine-type endopeptidase activity; cathepsin S activity; peptidase activity; hydrolase activity |
| MSP21 | AK004119.1 | 1429348_at | 159,2 | 504,7 | 799,9 | secreted, semaphorin E, neuroscience |
| MSP22 | BF148029 | 1431079_at | 59 | 60,8 | 248 | secreted, C1q and tumor necrosis factor related protein 2, Complement component C1q domain. Globular domain |
| MSP23 | BB475194 | 1456404_at | 143,1 | 435,7 | 389,3 | secreted, a disintegrin-like and metalloprotease (reprolysin type) with thrombospondin type 1 motif, 5 (aggrecanase-2) |
| MSP24 | AU067747 | 1433529_at | 59,2 | 155,1 | 332,9 | secreted, Calcium-binding EGF-like domain, have role in skeletal muscle development |
| MSP25 | AI507307 | 1459897_a_at | 138,9 | 145,7 | 381,6 | secreted, suprabasin, some role in the process of epidermal differentiation |

MSP05 is an evolutionarily conserved small putative secreted protein of unknown function (**Fig. 27a,b**), and it was described that its message is selectively expressed in $CD133^+$ and $CD\ 34^+$ cells (Jaatinen et al., 2006; Liu et al., 2000b).

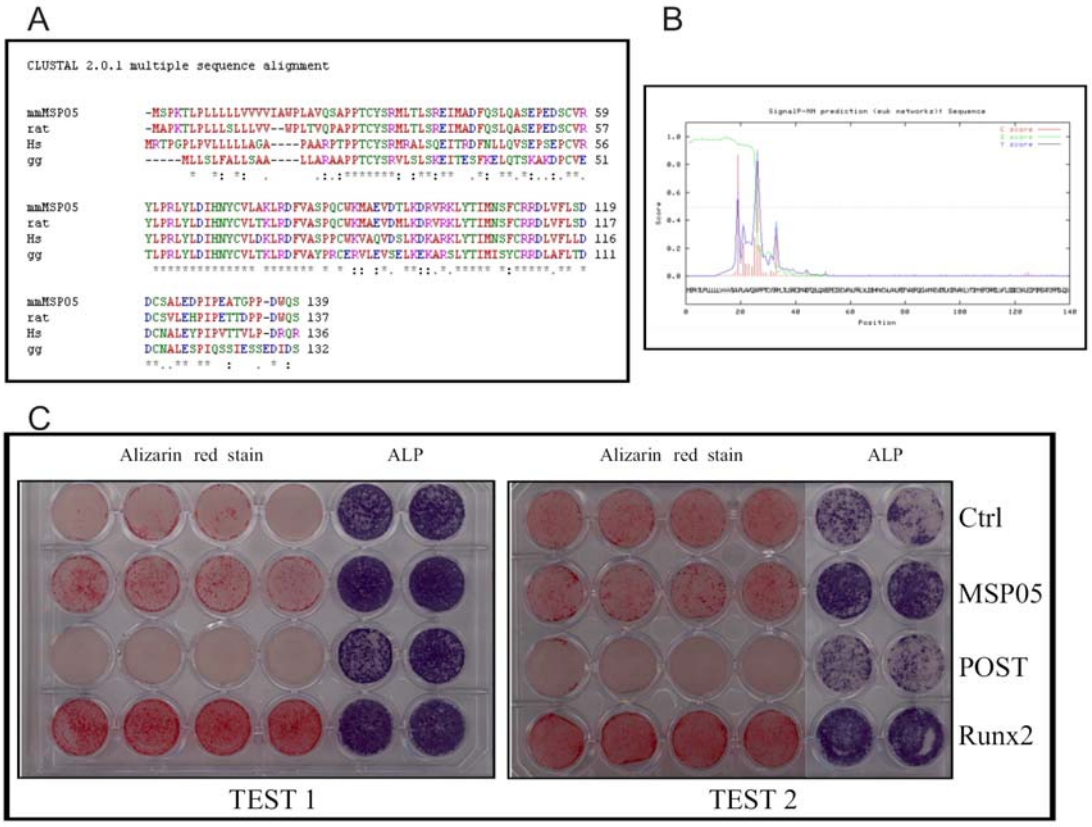


**Fig. 27.** Msp05 mildly induced mineralization in chBM. (A) The alignment of MSP05 proteins from different species. (B) SignaIP prediction using MSP05 protein sequence indicated that MSP05 is potentially a secreted protein. (C) In vitro test for bone mineralization. After switching into stimulation medium containing 10mM beta-Glycerophosphate and 50μg/ml Ascorbic acid, as a positive Ctl, chBM infected by Runx2 virus went mineralization quicker and stronger (lower panel); as a negative Ctl, chBM infected by SCYL1BP1 virus slowed down the mineralization process, indicated by Alizarin red staining (the third layer panel). Compared with chBM without virus infection or infected by GFP virus (Ctl), chBM infected by Msp05 virus showed mild induction of mineralization, indicated by both Alizarin red staining and alkaline phosphatase (ALP) activity (upper 2 layers). Two independent tests are shown.

Bone development and homeostasis are dependent on various types of secreted proteins. As an independent part, however, partially serving GO project, our gene chip data analysis identified a novel secreted factor likely involved in endochondral ossification. However further study is needed to fully address its function.